smart cities

MDPI

Article

Performance Evaluation of Small Wind Turbines Under Variable Winds of Cities: Case Study Applied to an Ayanz Wind Turbine with Screw Blades

Gonzalo Abad *, Ander Plaza and Gorka Kerejeta

Computer and Electronics Department, Mondragon University, 20500 Mondragon, Spain; ander.plaza@alumni.mondragon.edu (A.P.); gkerejeta@mondragon.edu (G.K.)
* Correspondence: gabad@mondragon.edu

Highlights:

What are the main findings?

- It is found how small-wind turbines behave in terms of energy production under the variable winds of city locations.
- It is found how it affects the power conversion system and control of small-wind turbines to the maximisation of energy production of small wind turbines.

What are the implications of the main finding?

- Thanks to these findings or analysis, it is possible to know for a given small wind turbine morphology if a low-cost and simple power conversion configuration can produce more energy than a typical and more complex and expensive Maximum Power Point Tracking (MPPT) based power conversion configuration.
- Therefore, knowing this, it is possible to design more cost-effective wind turbines than traditional ones.

Abstract: Small wind turbines placed at city locations are affected by variable-speed winds that frequently change direction. Architectural constructions, buildings of different heights and abrupt orography of Cities make the winds that occur at City locations more variable than in flat lands or at sea. However, the performance of Small-wind turbines under this type of variable wind has not been deeply studied in the specialised literature. Therefore, this article analyses the behaviour of small wind turbines under variable and gusty winds of cities, also considering three types of power electronics conversion configurations: the generally used Maximum Power Point Tracking (MPPT) configuration, the simple only-rectifier configuration and an intermediate configuration in terms of complexity called pseudo-MPPT. This general-purpose analysis is applied to a specific type of wind turbine, i.e., the Ayanz wind turbine with screw blades, which presents adequate characteristics for city locations such as; safety, reduced visual and acoustic impacts and bird casualties avoidance. Thus, a wide simulation and experimental tests-based analysis are carried out, identifying the main factors affecting the maximisation of energy production of small wind turbines in general and the Ayanz turbine in particular. It is concluded that the mechanical inertia of the wind turbine, often not even considered in the energy production analysis, is a key factor that can produce decrements of up to 25% in energy production. Then, it was also found that electric factors related to the power electronics conversion system can strongly influence energy production. Thus, it is found that an adequate design of a simple pseudo-MPPT power conversion system could extract even 5% more energy than more complex MPPT configurations, especially in quickly varying winds of cities.

Keywords: small-wind turbines; variable wind speed; wind at city locations; power conversion configuration; Maximum Power Point Tracking (MPPT); Ayanz wind turbine with screw blades; equivalent inertia

check for updates

Citation: Abad, G.; Plaza, A.; Kerejeta, G. Performance Evaluation of Small Wind Turbines Under Variable Winds of Cities: Case Study Applied to an Ayanz Wind Turbine with Screw Blades. *Smart Cities* **2024**, *7*, 3241–3288. https://doi.org/10.3390/smartcities7060126

Academic Editor: Pierluigi Siano

Received: 9 September 2024
Revised: 24 October 2024
Accepted: 28 October 2024
Published: 30 October 2024

Copyright: © 2024 by the authors. Licensee MDPI, Basel, Switzerland. This article is an open access article distributed under the terms and conditions of the Creative Commons Attribution (CC BY) license (https://creativecommons.org/licenses/by/4.0/).

1. Introduction

In this day and age, global warming and climate change have become critical problems which demand innovative and sustainable solutions in the energy field. This situation has prompted a transition towards renewable energy sources with the objective of reducing greenhouse gas emissions and promoting cleaner and safer electricity generation [1,2]. Generally, this transition has been dominated by large solar power installations, and the solar photovoltaic market has evolved from 70 GW in 2011 to 942 GW in 2021 [3]. Nevertheless, in recent years, interest has grown in self-consumption technologies which will allow individuals and communities to generate their own electricity. This fact causes a decrease in their dependence on the conventional electrical network [4].

Solar photovoltaic energy has been the predominant technology in this area due to the maturity of the market, the decreasing cost of solar panels, and the ease of installation in urban and residential environments [5]. However, small-scale wind energy (small wind turbines, SWT) is becoming a complementary option [6]. This type of energy has lots of advantages, especially in regions where wind resources are abundant and solar conditions are not as good as others. Also, while the PV panels work well in summer, their efficiency downgrades the rest of the year. For the wind turbines, the situation is different, as the sun does not affect them; they give a more regular energy quantity during the year [7]. Despite the growing interest in these technologies, research in SWTs has not so evolved, and there are few studies that have extensively analysed their performance in real urban wind conditions.

In general, smart cities require a lot of studies to be conducted. For instance, in [8], a study is made around the energy management in residential microgrids; in [9], a study in data-driven reliability prediction for district heating networks is made; and in [10], research is performed on characterising smart cities based on artificial intelligence. As a result of all these studies and the evolution of smart cities, the development of urban wind turbines presents multiple technical and economic challenges. First, it is essential that these turbines are cost-effective compared to the PV technologies, which have seen an appreciable cost reduction over the last decade. This cost has fallen to the point that to produce 1 W, only $0.5 USD is needed [11]. Moreover, it is very important that SWTs offer stable and efficient performance in urban wind conditions, which are often turbulent and with fluctuating speeds [12]. Although interest in these technologies is growing, no further research has been conducted on SWTs, and few studies have been performed on their performance in real urban conditions [13].

A very important part of wind turbines is the power generation conversion system. Depending on this power electronic circuit, a given wind turbine morphology is able to extract more or less power from the wind. There are 3 main power configurations which are going to be analysed in this article: only rectifier topology, pseudo-MPPT topology and MPPT topology [14]. The reason for analysing these is that no research has been conducted about which of the three is the best. Furthermore, no research has been performed to test all of them against urban wind environments and, more specifically, against different urban wind environments in changing conditions [15]. Also, little research has been conducted about which of the two main turbine topologies is the best for city environments (VAWT or HAWT) [16,17]. The objective is also to give data and information about this topic.

Then, focusing on this mentioned topic and with the idea for the commercial development of the small wind turbine research topic, one of the patents granted in 1606 to the distinguished inventor Jerónimo de Ayanz y Beaumont from Spain has been taken as a design reference [18,19]. This patent claims the use of a wind turbine based on screw blades, with a structure around it to channel or enclosure the wind. Having this known and using a commercial wind turbine based on Archimedes screw blades (Liam F1 AMW-750-D-150W, ref. [20]), a built Ayanz wind turbine has been used for all the tests. This blade morphology has been widely studied, for instance, in [21–25]. Besides, this topology has been used due to its positive aspects such as its Cp value, noise reduction (due to relatively low rotation speeds), start-up and operation at low wind speeds, ease of construction, visual impact (due

to the tube) and the avoidance of bird deaths due to the frontal net mounted on it [26]. This mentioned wind turbine can be seen in Figure 1. Knowing this, it has been decided to test this wind turbine in different wind gust scenarios based on real wind measurements taken in the urban area of Mondragon City (different speeds, orientations and repetitive gusts).

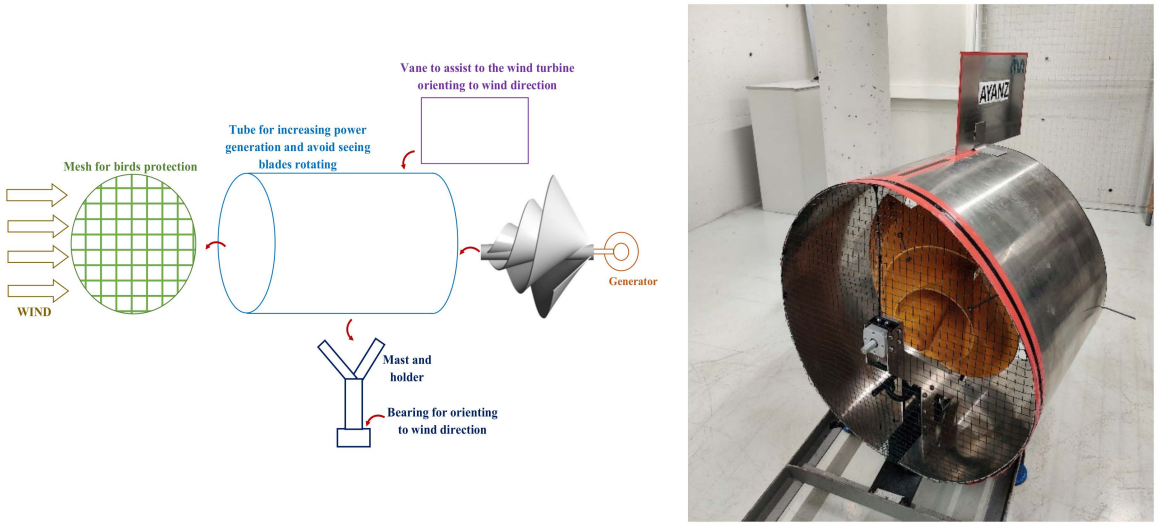

Figure 1. The Ayanz Wind Turbine with Screw Blades. (**a**) Graphical scheme showing its main parts, (**b**) Prototype developed at Mondragon University, based on the commercially available Liam F1 AMW-750D-150W wind turbine and a cylindrical enclosure made of aluminium [20].

Finally, it is important to highlight that although there are other studies that have explored the design and application of SWTs in urban environments, none has addressed the performance analysis with real urban wind data as specifically as the present work [27]. This analysis aims to fill a significant gap in the current literature, providing a solid foundation for future research and development of small-scale wind technologies that are truly effective and sustainable in the field of urban self-consumption [28,29]. Hence, one of the major contributions of the article, which was not addressed in related field papers, is bringing in real wind measurements of urban cities to analyse the energy production of wind turbines. It is almost impossible to find research articles that employ such long real wind data with a sample time of 1 s to quantify energy production. A second remarkable contribution of this article is the demonstration that the inertia of the wind turbine is a key factor in determining the capacity to maximise the energy generated by the wind. Later, it is shown that turbine designs with oversized inertia proportionally reduce their capacity to extract energy from winds of urban areas (gusty winds). Thus, high-inertia turbine designs can decrease up to 25% of the energy production compared to light or low-inertia turbine designs (see sub-sequent Section 4). After that, a third contribution of the paper is the fact that it demonstrates which factors influence the power electric conversion system and control of small-wind turbines to the maximisation of their energy production. Among the most common power electronic generation configurations employed in wind turbines, it is demonstrated that low-cost and reliable power conversion configurations (pseudo-MPPT and Only-Rectifier configurations) can produce more energy than a classic and more expensive Maximum Power Point Tracking (MPPT) based power conversion configuration. In fact, it is shown that the pseudo-MPPT with passive external capacitances proposed in this article can be suitable for increasing around 2% of energy production in wind turbines with peaked Cp curve characteristics). Finally, in the last section, practical simplified inertia mathematical expressions are provided for most typical wind turbine morphologies. Thanks to them and knowing the geometrical dimensions of a given turbine, it is easy to calculate a first approach of the equivalent inertia, for later knowing its estimated energy

production at gusty winds. With the help of these expressions, it is shown that horizontal axis wind turbines can present 2 or 3 times less inertia than vertical axis wind turbines, with the same incident wind area. To conclude, experimental results validate the main contributions and findings of the article.

2. Horizontal Axis Wind Turbine Used in This Study

2.1. The Ayanz Wind Turbine with Screw Blades

As commented earlier, the original patent of Ayanz inventor, published in the year 1606 [18,19], provides us with a horizontal axis wind turbine with screw blades and then blades within an enclosure with a cylindrical shape. This cylindrical enclosure allows the capacity of the blades to capture more energy from the wind [26], together with some other practical advantages. Figure 1 graphically illustrates the wind turbine prototype developed at Mondragon University, using the commercially available Liam F1 AMW-750D-150W wind turbine. It uses the well-known Archimedes Spiral Wind Turbine [30] as a screw-bladed wind turbine.

This is a horizontal-axis wind turbine, so it needs to be oriented in the direction of the wind. A very quick and effective orientation is achieved with this turbine, thanks to the assistance of the vane located at the bottom of the cylindrical enclosure, together with the fact that this turbine, due to its morphology and geometry, tends to self-orientate.

2.2. Main Characteristics of This Wind Turbine

The cylindrical enclosure of the wind turbine enables the incorporation of a metallic mesh at the input, preventing birds from entering the inside of the wind turbine. This effective protection mesh prevents potential damage to the birds. In [26], it has been experimentally tested and demonstrated that if the mesh is sufficiently thin, it does not reduce the capacity of the turbine to capture energy from the wind, not affecting its efficiency and aerodynamic coefficients. Then, thanks to the tube also, the visual impact and noise produced by the wind turbine are reduced. It should be noted that this enclosure considerably reduces the fact to continually see and hear the blades rotating, which is a fairly important benefit for many potential users who will install wind turbines on the roofs of their homes. Finally, the tube also brings another advantage, which is protection from potential damage to the blades. Note that if one blade is accidentally broken, the safety of people or objects near the turbine is guaranteed since the blade would not exit the tube. All these advantageous characteristics are summarised in Table 1. On the other hand, the turbine presents the following geometrical characteristics [26]: 3 blades, effective radio of blades = 37.5 cm, radio of the tube = 40.75 cm, longitude = 60 cm, while the electric characteristics of the Permanent Magnet Synchronous Generator are: parasitic resistance = 9.56 Ω, parasitic inductance = 20.96 mH, ϕ_{pm} = 0.2665 Wb, pole pairs = 6.

Table 1. Main practical advantageous characteristics of the Ayanz Wind Turbine based on Screw Blades (at the end of the article, these characteristics are further explained and compared to other wind turbine morphologies).

Main Characteristic
It presents considerably high Cp coefficient so it is able to capture a significant portion of energy from the wind
reduction of the noise impact due to the tube and its moderately low rotational speed operation
minimization of the blades being watched rotating due to the tube
casualties in birds elimination due to the mesh
Safety provided by the tube since it protects from potential damages at the blades
Very fast Auto orientation due to its effective weathervane placed outside the blades

To conclude, it has to be remarked that this wind turbine has been chosen for the study provided in this article, not only due to its above-mentioned benefits but also because it is a horizontal axis wind turbine that needs to be oriented to the wind direction. As will be later shown, a study is carried out in the article, showing how the time the wind turbine needs to be oriented to the wind direction impacts the produced energy. Finally, it has to be remarked that for city locations, this is one of the safest small wind turbines available (for surrounding objects, animals or persons) and also considerably reduces visual and acoustic impact, which are determinant factors in placing small wind turbines at city locations where many people live nearby.

3. Power Conversion Configurations

3.1. Power Circuits and Controls

This section shows the three power conversion configurations for small wind turbines analysed in this paper [26]. These three power conversion systems are shown in Figure 2. The most general and complete conversion systems are presented in the figure above. It connects directly a diode-based rectifier to the AC generator, then a DC-DC conversion stage facilitates the implementation of a Maximum Power Point Tacking Algorithm (MPPT), and finally, the electrical power generated is transmitted to a second stage, which could be a battery, the electric AC grid or even a DC grid. For the MPPT consecution, a specific control algorithm is presented in the next sub-section, and consequently, a microprocessor enables its implementation.

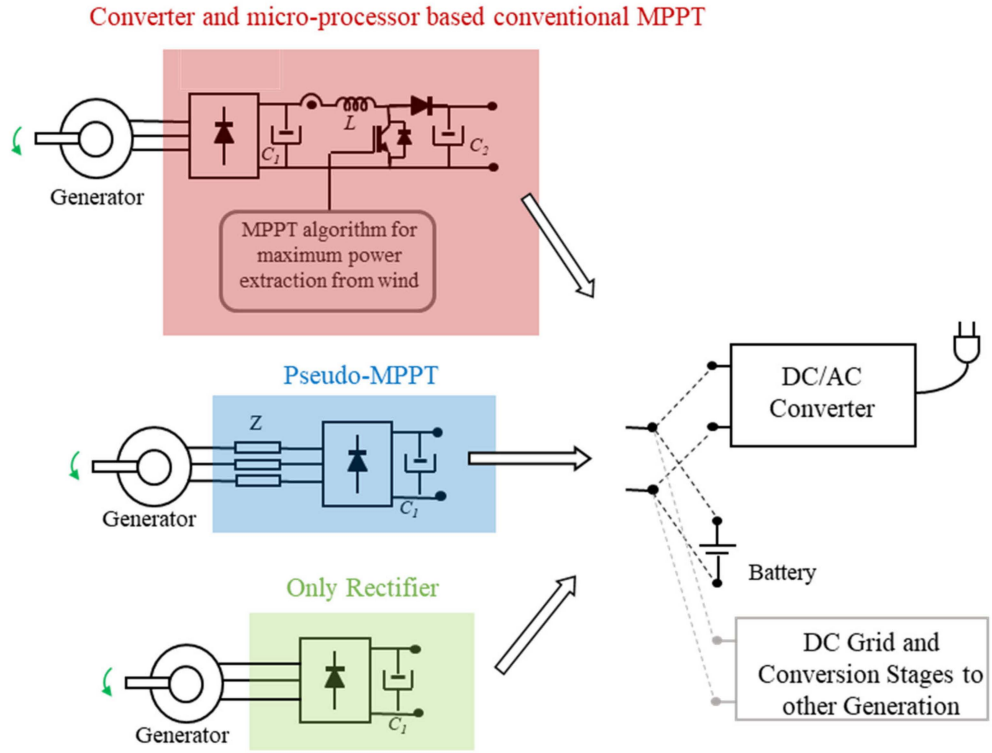

Figure 2. Most common power conversion configurations for small wind turbines [26].

Then, in Figure 2 below, another power conversion system is presented, which is based only on a diode-based rectifier and a DC capacitor for smoothing the output DC voltage. Compared with the previous configuration, this is a much simpler conversion concept since no DC-DC conversion system is used and, therefore, no microprocessor is required. This type of conversion system is traditionally oriented to the smallest wind turbines and to low-cost wind turbine concepts.

Finally, a concept that is somewhere in the middle of the previous two in terms of complexity is the one called a pseudo-MPPT conversion system, and it is shown in

the middle in Figure 2. As can be noticed again, it incorporates a diode-based rectifier, the smoothing capacitor and an additional impedance that could be an inductance or a capacitance [26]. This concept is tentatively conceived to be able to extract more power from the wind than the Only-Rectifier but less than the Conventional or Ideal MPPT, with a power conversion system that does not require a microprocessor, therefore reducing the complexity and losses of the power conversion system. This fact is schematically represented in Figure 3, where it is seen that at steady-state and constant wind speed conditions, theoretically, the Ideal MPPT is able to make the turbine operate at the peaks of the power curves at each wind speed (V_w). However, the Only-Rectifier concept, since it operates at almost constant rotational speed (due to the nearly constant voltage operation of the generator imposed by the battery), is not able to work at the peaks of the power curves, generating less power. Finally, the pseudo-MPPT concept, thanks to the voltage droop at the impedance located at the output terminals of the generator, produces a slight variation in the voltage seen by the generator, also producing a slight variation of the mechanical speed, tentatively following better the power peaks of the power curves, as depicted in Figure 3. In subsequent analyses of the paper, for simplicity purposes, it will be supposed that the electric energy generated by the small wind turbine is evacuated to a battery. As can be noticed, the left situation in Figure 3 shows a 'low voltage' battery chosen ('low' speed) for pseudo-MPPT and Only Rectifier. On the contrary, the Right situation shows a 'high voltage' battery chosen ('high' speed) for pseudo-MPPT and Only Rectifier. In the left situation, the pseudo-MPPT needs to increase the speed with higher winds, while in the right situation, the pseudo-MPPT needs to decrease the speed with higher winds. Both situations are possible, depending on how all the elements of the system are chosen.

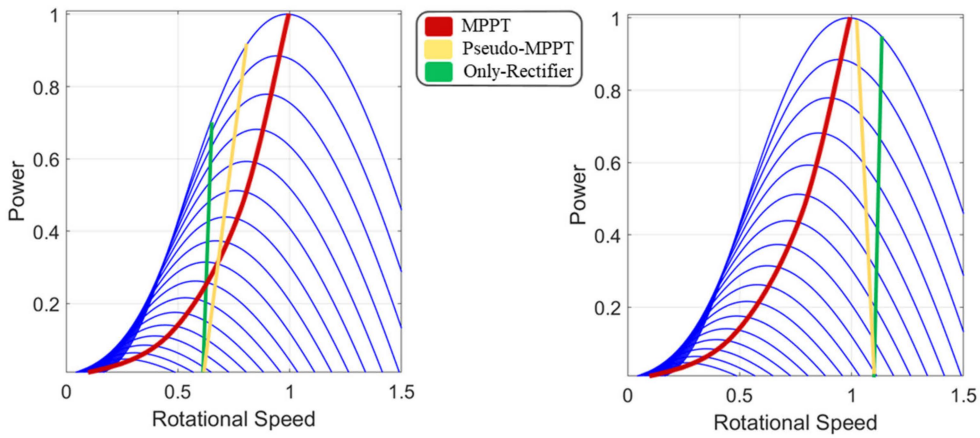

Figure 3. Power generated with the same wind turbine using the three power conversion configurations studied in this paper. The left situation shows a 'low voltage' battery chosen ('low' speed) for pseudo-MPPT and Only Rectifier. The right situation shows a 'high voltage' battery chosen ('high' speed) for pseudo-MPPT and Only Rectifier. Curves in blue, represent power at different wind speeds.

3.2. Indirect Speed Control Based Conventional-MPPT

This section roughly explains how the Conventional-MPPT works in small wind turbines. There are several MPPT control algorithm versions [31], but in this article, a typically used one is used, i.e., the Indirect Speed Control Conventional-MPPT [32,33]. The control block diagram is depicted in Figure 4.

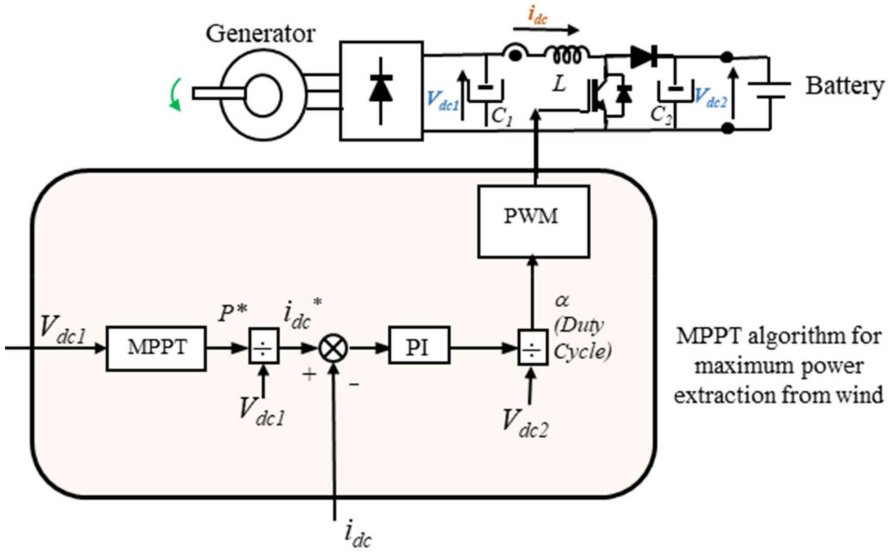

Figure 4. Indirect Speed Control based MPPT [32,33].

It is seen that the control generates the pulses for the controlled switch of the DC-DC converter. It depends on how the elements of the specific system are designed, but in general, a Boost DC-DC converter is employed that increases the DC voltage from the input V_{dc1} to V_{dc2} by means of the well-known equation:

$$\frac{V_{dc2}}{V_{dc1}} = \frac{1}{1-\alpha} \tag{1}$$

Being α the duty cycle for the controlled switch, and V_{dc2} is imposed by the battery employed. This MPPT control creates these pulses by only measuring two variables: V_{dc1} and i_{dc}. The fact that it avoids the need to measure the rotational speed with a sensor is advantageous for the simplicity and reliability of practical and successful wind turbines.

Then, the AC generator, which normally is a Permanent Magnet Synchronous Generator, converts the mechanical energy extracted by the turbine from the wind into electric energy. The single-phase equivalent circuit of the Synchronous Generator is depicted in Figure 5.

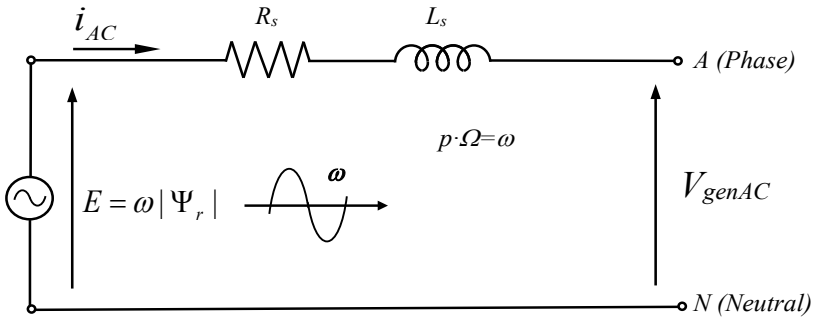

Figure 5. Synchronous generator's single phase equivalent circuit.

As noticed, neglecting the voltage droop at the parasitic resistance and inductance of the generator, at its terminals, sinusoidal three-phase voltages appear with approximated amplitude (Phase-to-Neutral voltage):

$$|V_{gen}|_{LN} \cong \omega |\Psi_r| \tag{2}$$

These voltages are the input voltages of the diode-based rectifier, which converts the three-phase AC voltages into DC output voltage, as schematically represented in Figure 6.

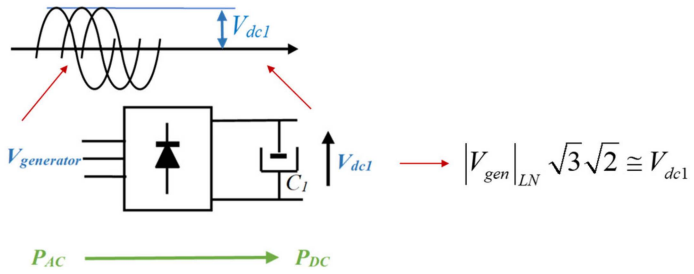

Figure 6. AC-DC conversion stage.

Thus, the DC voltage that appears at the input of the DC-DC converter is approximately as follows:

$$V_{dc1} \cong p\Omega|\Psi_r|\sqrt{3}\sqrt{2} \tag{3}$$

Which is indeed a voltage that is proportional to the rotational speed. Thus, taking advantage of this fact, the speed sensor is avoided.

Then, as commented before, the speed of the control performed by this MPPT version is an indirect speed control version. Thus, the rotational speed of the turbine is controlled indirectly without a speed sensor. The generator is in charge of imposing an electromagnetic torque T_{em}, which follows the maximum power points curve ($T = k\Omega^2$ and $P = k\Omega^3$). The torque created by the turbine, T_t, follows the turbine torque curves at different wind speeds, as illustrated in Figure 7. Consequently, the turbine naturally reaches a steady-state equilibrium at a rotational speed that follows the maximum points of the power curves.

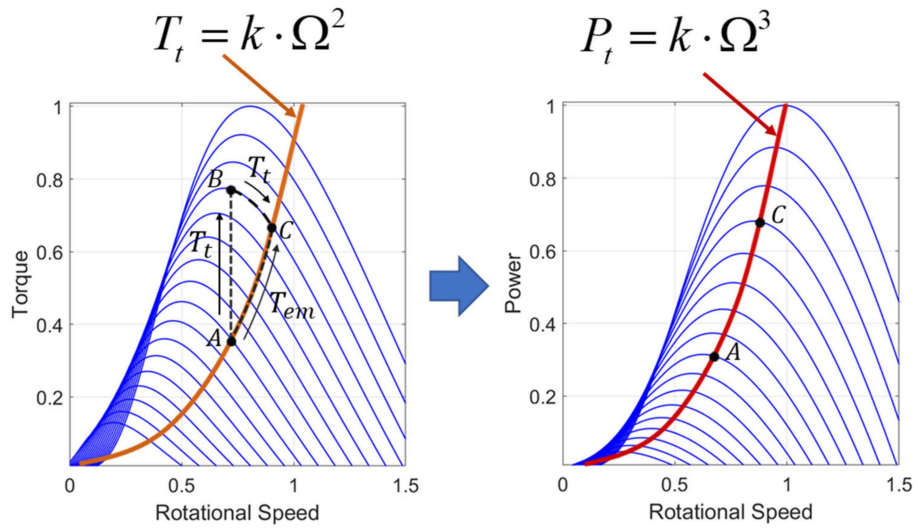

Figure 7. Indirect speed control of the wind turbine by imposing an electromagnetic torque T_{em}, which follows the maximum power points curve [32,33]. T_t follows a trajectory that goes through points A, B and C.

Hence, the electromagnetic torque T_{em} is controlled by controlling the power as illustrated in Figure 8 (note that power and torque are related by the rotational speed, and if one is controlled, the other is too).

Thus, knowing what has been exposed before, the power generated can be mathematically expressed as:

$$P = k \cdot \Omega^3 = k \cdot (V_{dc1} \cdot k')^3 \tag{4}$$

Being k' deduced from previous Equation (3):

$$\Omega \cong V_{dc1} \frac{1}{p|\Psi_r|\sqrt{3}\sqrt{2}} = V_{dc1}k' \tag{5}$$

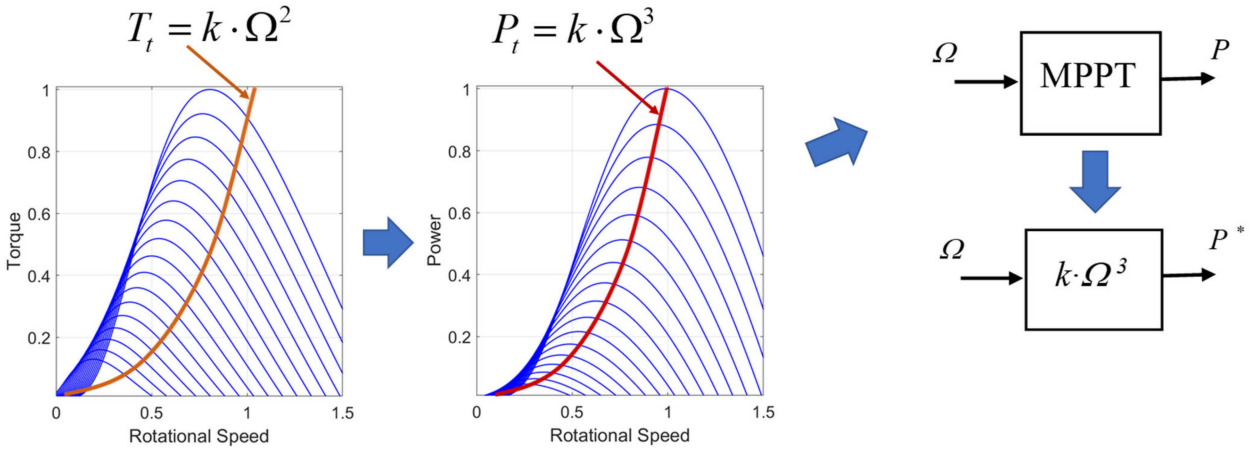

Figure 8. Controlling the power, the electromagnetic torque T_{em} is controlled.

Resulting at the MPPT's power reference strategy shown in next Figure 9. Then, the power is controlled (which means controlling the electromagnetic torque T_{em}) by controlling the i_{dc} with its corresponding control loop, as shown before in Figure 4.

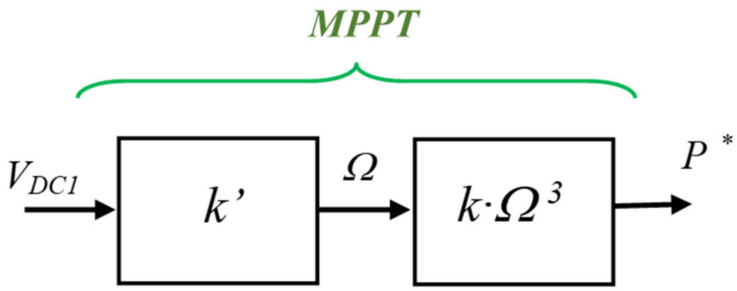

Figure 9. MPPT with power reference generation without using a speed sensor.

3.3. Only-Rectifier and Pseudo-MPPT Configurations

The power configurations analysed in this section are simpler than the previous one. Thus, for instance, Figure 10 first shows the generation power curve obtained with only-rectifier configuration. This is a nearly constant rotational speed and nearly perpendicular curve since the battery imposes a constant amplitude voltage at the terminals of the generator. In practical generator designs of Small Wind Turbines, the parasitic resistance and inductance (R_s and L_s) are quite significant. Therefore, the power curve obtained presents a big positive slope (near 90°), as shown in Figure 10. Consequently, the generated power at each wind speed is not at the peak of the turbine's power curve, extracting at steady-state constant wind less power than the conventional MPPT seen in the previous sub-section.

Then, the proposed pseudo-MPPT in [26] incorporates an impedance that, in most cases, is an inductance, but there could be situations where capacitance would be more suitable. Hence, in Figure 11a, the simplified single-phase equivalent electric circuit of the system with inductive impedance is illustrated. From this electric circuit, in Figure 11b, it is shown how the space vector diagram of the fundamental components of the voltage and currents are. In addition, how the MPPT power curve is moved with different L values is also shown. In general, the fundamental components of the rectifier's input voltage (imposed by the voltage of the battery) and the current are nearly in phase, as shown. This fact shows that the emf voltage at which the equilibrium is reached is bigger than the rectifier's voltage. And indeed, this difference is bigger with bigger AC currents (bigger generated powers). This produces, as commented before, generated power curves with a positive slope near 90°. This slope can be made smaller by increasing the included impedance L, as depicted in Figure 11b.

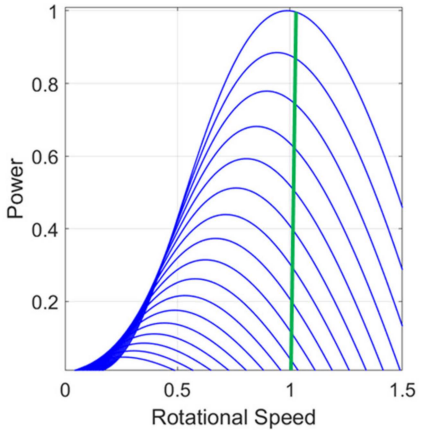

Figure 10. Generation power curve obtained with only-rectifiier configuration, achieving nearly constant rotational speed, and a nearly perpendicular curve. Note that in this graphical example, by choosing an appropriate DC voltage battery, a rotational speed was chosen that nearly obtained 1 p.u. power at 1 p.u. speed. This adequation is not always possible since it depends on the system elements available, such as the generator's characteristics, turbine, batteries, etc.

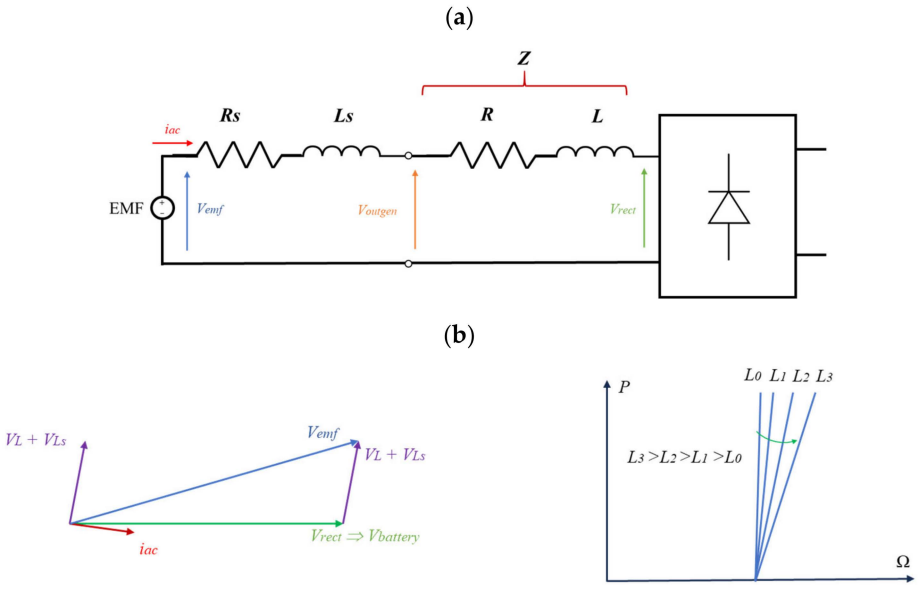

Figure 11. (**a**) Simplified single-phase equivalent electric circuit with inductive impedance in pseudo-MPPT concept. (**b**) Space vector diagram of the fundamental components of the voltage and currents and how the pseudo-MPPT power curve is moved with different L values.

On the other hand, depending on how much the voltage of the battery is chosen, the parasitic impedances of the generator (R_s and L_s) and the wind turbine's characteristics, it could be interesting to make the slope of the generated power curve closer to positive 90° or even in some cases, make the slope bigger than 90°. This fact can be achieved, as illustrated in Figure 12a,b, by including an external capacitance, which compensates for the voltage drop of the parasitic inductance L_s of the generator.

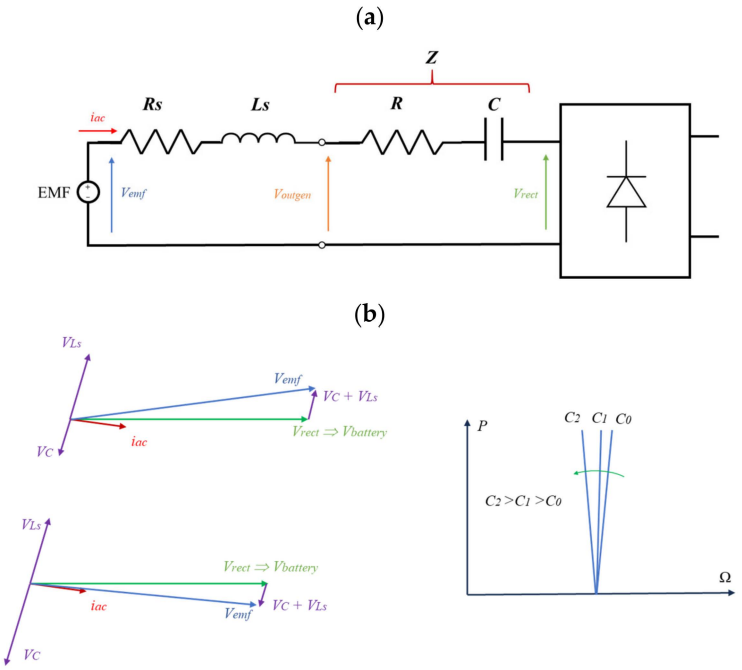

Figure 12. (**a**) Simplified single-phase equivalent electric circuit with capacitive impedance in pseudo-MPPT concept. (**b**) Space vector diagram of the fundamental components of the voltage and currents and how the pseudo-MPPT power curve is moved with different C values.

4. Computer-Based Simulation Analysis

4.1. Wind Measurements at City Locations

In this subsection, several wind patterns measured in the urban area of the City of Mondragon are presented. These measured wind measurements are later used in subsequent simulation analyses and are also the base for the experimental results developed in the later section as well. Hence, an anemometer is placed on the terrace of the 11th building of Mondragon University in Mondragon City. The anemometer and the location of the building are shown in Figure 13. The anemometer is a WMS-21 Wind Station of Omega manufacturer (1800 Industrial Center Circle, Charlotte, NC, USA) whose wind measurements have been calibrated and contrasted with another portable XA1000 Lufft anemometer (Fellbach, Germany) to ensure accuracy. The location of the anemometer could also be a suitable place to install a real small wind turbine for electric energy generation purposes. However, in this article, the authors could not have installed a wind turbine due to practical and administrative issues. By having and analysing the wind measurements at this location, it is also a representative model of many other similar roofs and terraces of different cities, where wind patterns with similar characteristics and behaviours are expected.

Thus, Figures 14–16 show several wind measurements with a sample time of 1 s on different days at this city location. Figure 14 corresponds with a low wind day, which is the most common wind pattern at the site. Then, Figure 15 represents a moderate wind day, which less often occurs than the previous pattern. Finally, Figure 16 shows an extremely windy day that occurs around no more than 5 days per year. In addition, it must be highlighted that the authors have realised many other wind measurements with portable anemometer XA1000 Lufft at different locations of this city and other cities, seeing that the wind patterns are always very similar. Thus, it can be noticed that the wind never is constant, at least in these types of city locations. The wind is gusty, almost always starting from a near zero wind speed and then increasing one or more times until one or several peaks are reached, to finally go down again until reaching a nearly zero wind speed again. Then, this gusty wind is repeated continuously. As can be inferred by carefully analysing Figure 14f, for instance, the duration of the time gusts can range from a few seconds to

several dozens of seconds. Therefore, it can be concluded that the real wind speed is continuously varying, which means that the small wind turbines placed at these locations that are affected by these winds need to adapt their rotational speed to these continuously varying winds (see previous section) in order to maximise the power extracted from these types of winds.

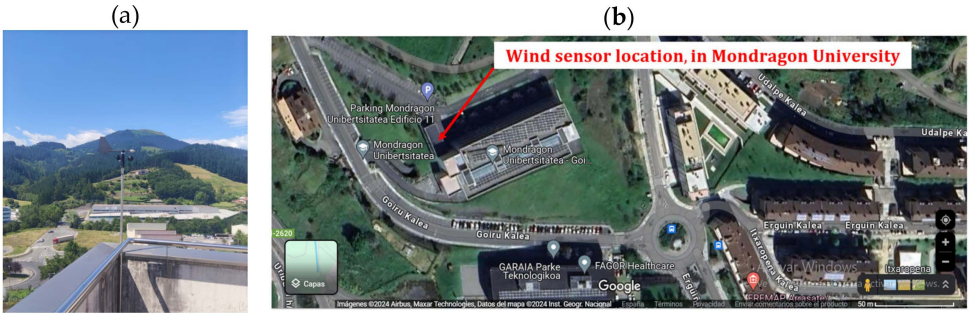

Figure 13. (**a**) WMS-21 Wind Station of Omega manufacturer (sample time = 1 s) located at the terrace of Mondragon University in the urban area of the City, (**b**) Google Maps photo showing where the anemometer has been placed for the study (place where the wind turbine can be located) at the 11th building of Mondragon University at Mondragon City.

The extraordinarily high wind measurements shown in Figure 16 are the less common ones at the site but are covered here as an illustrative example only.

Then, Figure 17a shows the probability density function of wind measurements (averaged every 10 min) between days 26th of September and 10th of October of 2024 at the location of the wind sensor (The Standard IEC 61400 [34] determines that a representative wind measurement of a particular site must be longer than 180 h and averaged 10 min wind speeds must be discretised every 0.5 m/s). It is measured that the average wind speed during these 15 days is 1.2 m/s, which is a quite low mean value. The same wind measurements corrected, for instance, to a 4 m higher location [34] are shown in Figure 17b. It is seen that the estimations predict an average wind speed of 1.68 m/s at this height. As can be noticed, the wind conditions of the site are quite poor if compared to locations where big mega-watt wind turbines are placed, in which averaged wind speeds are normally greater than 5 m/s. Urban Cities, due to their low heights and multiple architectural barriers, present these types of wind conditions.

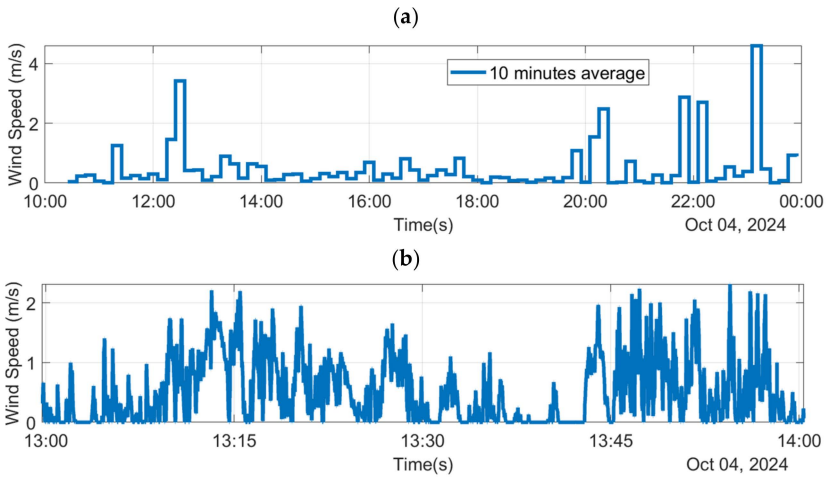

Figure 14. *Cont.*

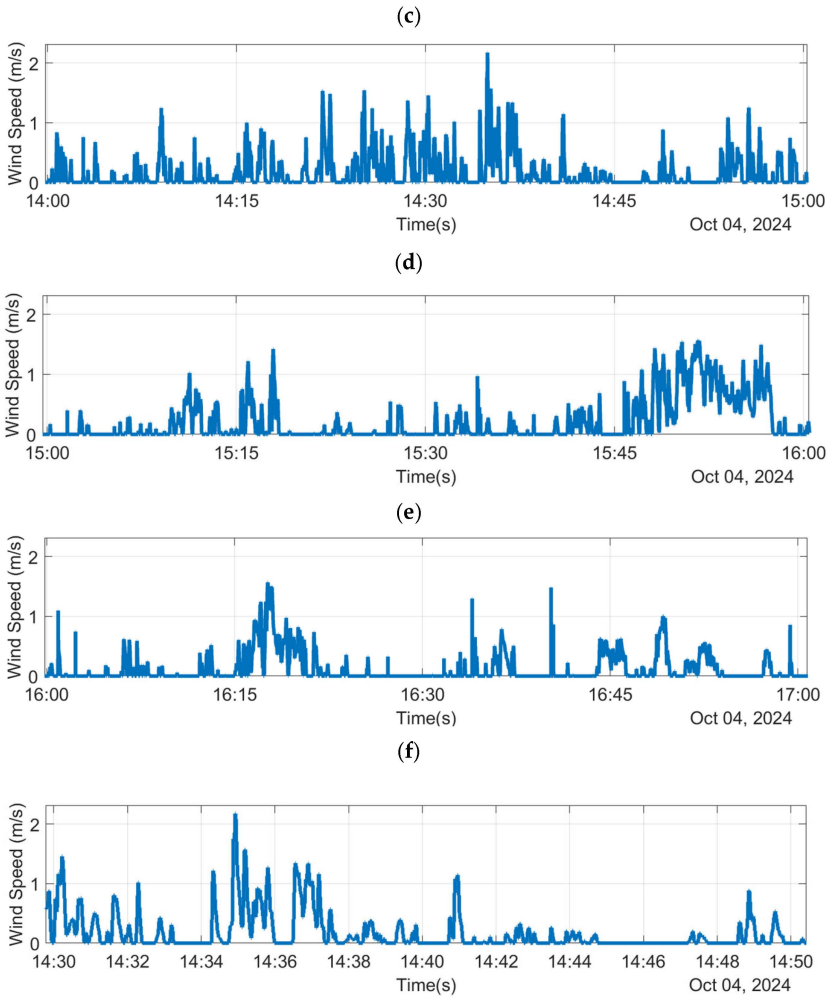

Figure 14. Wind speed measured with WMS-21 Wind Station (sample time = 1 s) at a low wind day (4th of October) in Mondragon University at the urban area of the City, (**a**) wind speed measurement during 12 h and averaged every 10 min, (**b**) wind speed measurement between 9:00 and 10:00 h, (**c**) wind speed measurement between 10:00 and 11:00 h, (**d**) wind speed measurement between 11:00 and 12:00 h, (**e**) wind speed measurement between 12:00 and 13:00 h, (**f**) wind speed measurement of 20 min showing the highest wind gust.

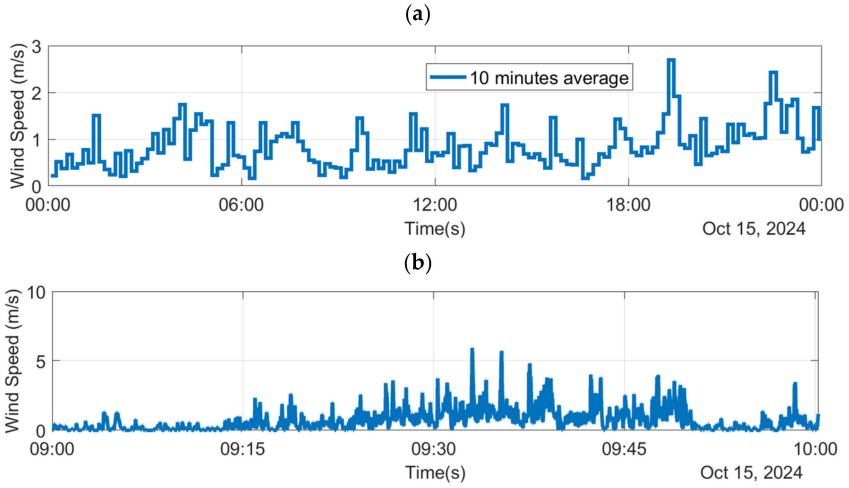

Figure 15. *Cont.*

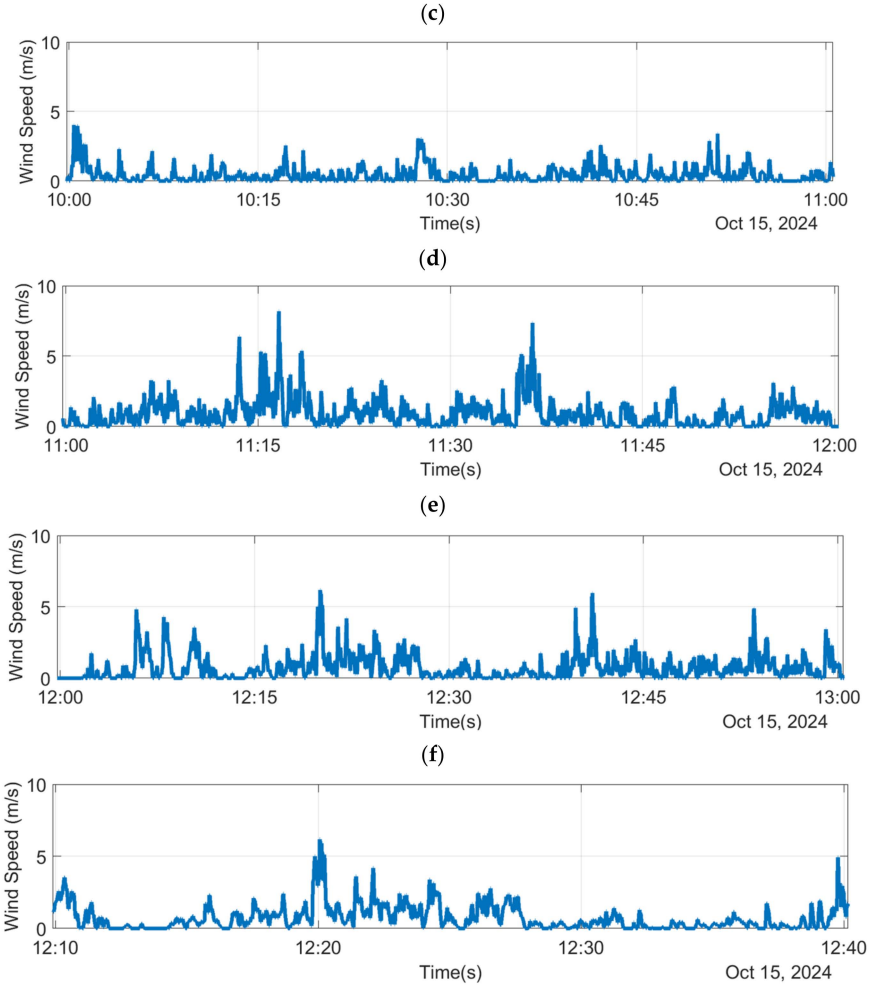

Figure 15. Wind speed measured with WMS-21 Wind Station (sample time = 1 s) at a moderate wind day (15th of October) in Mondragon University in the urban area of the City, (**a**) wind speed measurement during 12 h and averaged every 10 min, (**b**) wind speed measurement between 9:00 and 10:00 h, (**c**) wind speed measurement between 10:00 and 11:00 h, (**d**) wind speed measurement between 11:00 and 12:00 h, (**e**) wind speed measurement between 12:00 and 13:00 h, (**f**) wind speed measurement of 20 min showing the highest wind gust.

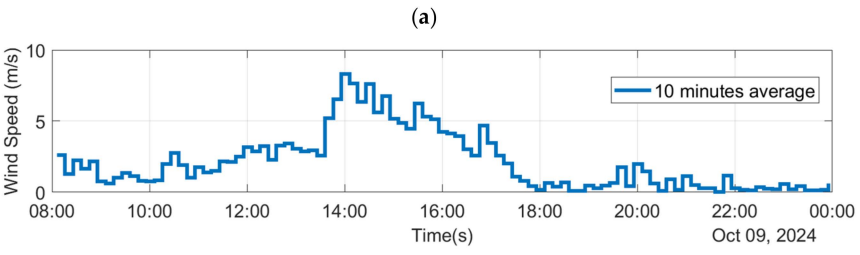

Figure 16. *Cont.*

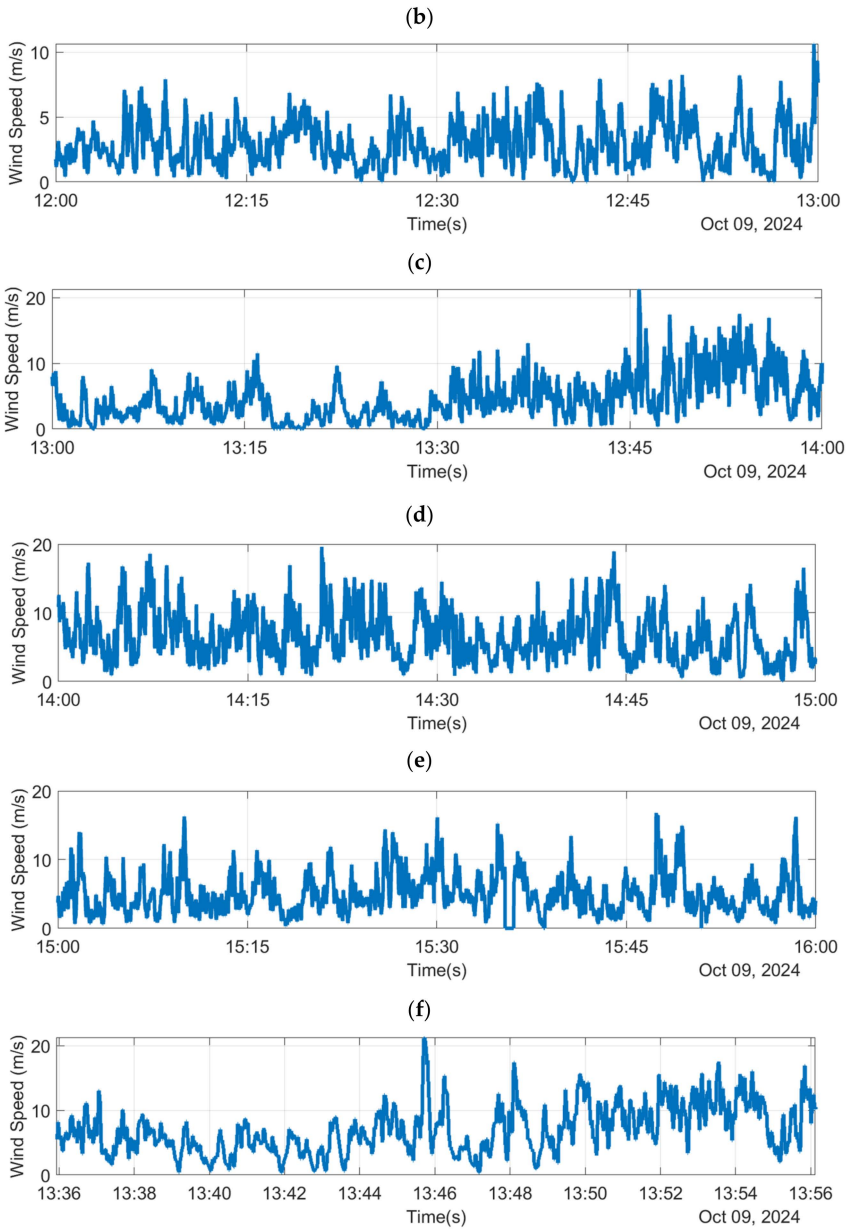

Figure 16. Wind speed measured with WMS-21 Wind Station (sample time = 1 s) at a very strong wind day ('Kirk' Storm on 9th of October) in Mondragon University at the urban area of the City, (**a**) wind speed measurement during 12 h and averaged every 10 min, (**b**) wind speed measurement between 12:00 and 13:00 h, (**c**) wind speed measurement between 13:00 and 14:00 h, (**d**) wind speed measurement between 14:00 and 15:00 h, (**e**) wind speed measurement between 15:00 and 16:00 h, (**f**) wind speed measurement of 20 min showing the highest wind gust.

4.2. Performance Analysis with Different Inertias

In this first set of analyses, it is important to understand how the inertia of the small wind turbines affects the maximisation of the energy generated. More specifically, how the gusty and continuously varying wind speed affects the efficiency of wind turbines with different inertia. For that purpose, a fictitious and idealised wind turbine will be used, with the Cp(λ) curve shown in Figure 18a. It represents an averaged Cp(λ) curve of the wind turbine that later is used in the experimental analysis, i.e., the Ayanz Wind Turbine based on Screw Blades. Note that this type of wind turbine presents a quite flat range at the higher values of the Cp curve, in the proximity of the optimum λ values where the maximum Cp is obtained.

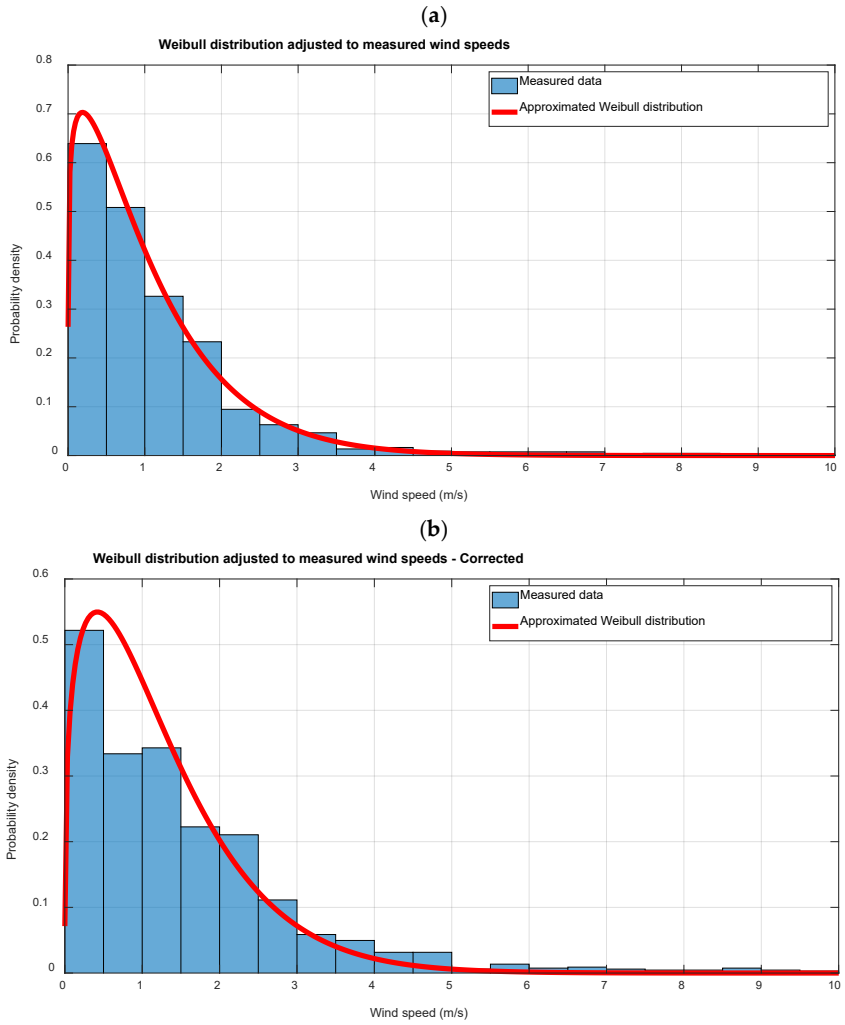

Figure 17. (**a**) The probability density function of wind measurements (averaged every 10 min and quantified every 0.5 m/s) between the 26th of September and the 10th of October. The approximated Weibull distribution function $f(v) = \left(\frac{k}{c}\right)\left(\frac{v}{c}\right)^{k-1} exp\left[-\left(\frac{v}{c}\right)\right]^{k}$ can be defined by k = 1.15, c = 1.1, and the average speed is 1.2 m/s. (**b**) Probability density function of the same wind measurements, after correction by the factor: $v_{meas}\left(\frac{z_{estim}}{z_{meas}}\right)^{\alpha} = \left(\frac{6}{2}\right)^{0.3} = 1.4$, which is an estimation of the wind measurement corrected to a 4 m higher location in an urban site [27]. The resulting parameters are k = 1.28 and c = 1.34, and the average speed is 1.68 m/s.

Then, Figure 18b shows the block diagram of the Matlab-Simulink model employed to perform an idealised MPPT operation of a wind turbine with different inertia. As can be noticed, a wind speed pattern excites the wind turbine modelled by means of the Cp(λ) curve. This idealised model provides the torque produced by the wind turbine Tt.

Then, the idealised MPPT explained in Section 3 generates the electromagnetic torque Tem produced by the generator-converter algorithm. Finally, both torques interact at the rotational shaft of the turbine, modelled by a simple inertia J. This inertia represents the sum of the shaft and generator and the dominant inertia of the wind turbine's screw blades. This idealised wind turbine model has been used in this analysis to decouple or avoid possible dynamic delays produced by realistic models of the generator, converter and control algorithm. By this approach, the MPPT's equation $T = k \cdot \Omega^2$ instantaneously provides the required electromagnetic torque (with no dynamic delay) to produce the maximisation of the generated power, i.e., to produce the MPPT. In this way, the affection of the inertia to the MPPT can be studied and decoupled from other turbines' characteristics or parameters.

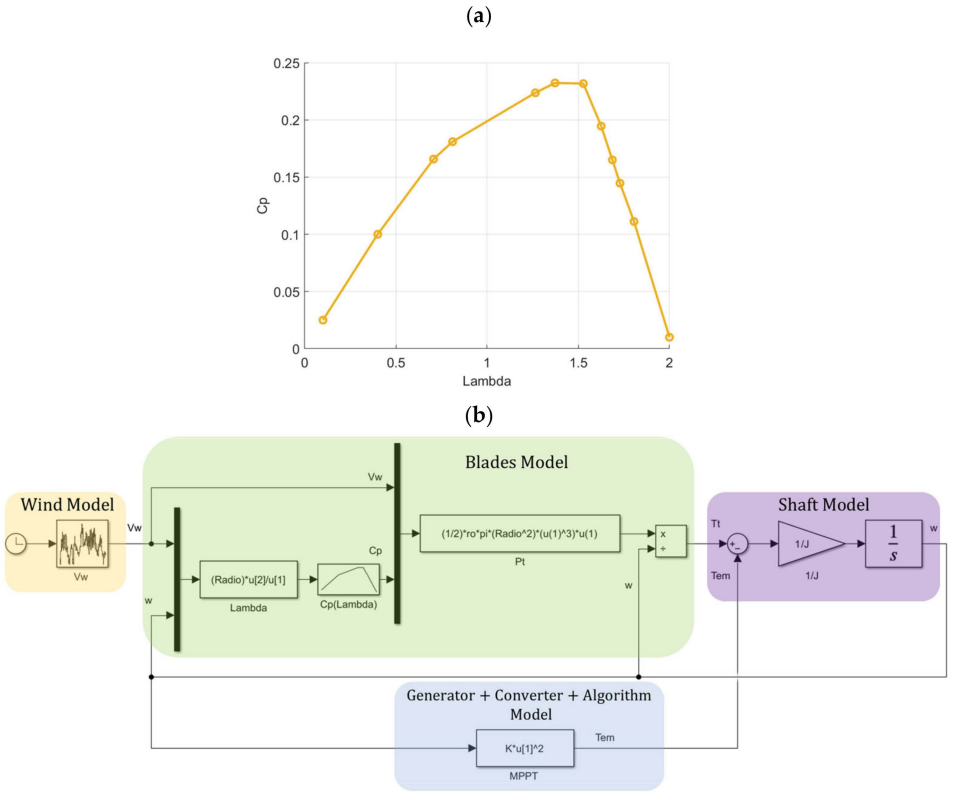

Figure 18. (**a**) Cp(λ) curve of the Ayanz Wind Turbine based on Screw Blades used for the first set of simulations analyses. (**b**) Block diagram of the Matlab-Simulink R2023b model to perform an idealised MPPT operation of wind turbine with different inertias.

Note that it could be possible to use a more realistic wind model or even more complex blades' and shaft models than the one depicted in Figure 18b, such as, for instance, incorporating stratifications phenomena, damping mechanical behaviours and others [35,36], however for simplicity purposes, these simple and very idealised models have been adopted which is enough to understand the effect of the inertia.

Hence, next Figures 19–21 show the performance of the Ayanz Wind Turbine based on Screw Blades with idealised Indirect MPPT control and three different inertia values; J = 0.03 kgm^2, J = 0.15 kgm^2 and J = 0.75 kgm^2. Using the same Wind speed pattern in all the cases, the obtained Tt and Tem performances, rotational speed, generated power, Cp and energy generated are shown. The different inertia simulated produced different performances in the three tests. In the first one in Figure 19, with very small inertia of the wind turbine, the idealised indirect MPPT control is able to follow quickly the gusts of the wind pattern studied, operating at optimum rotational speed during the experiment and, therefore, always producing the maximum achievable power at each wind speed and every instant. Therefore, during all the time, the turbine operates at a maximum Cp value of 0.23, with only exceptions at wind speeds of cero or very near to cero (at these moments, the achievable power from wind is zero). Under these circumstances, the obtained energy is the maximum available from this wind speed pattern, which is 1212.65 J.

Then, in the second experiment shown in Figure 20, with an inertia of J = 0.15 kgm^{2,} which is 5 times bigger than the previous case, the idealised MPPT control is not able to follow the wind speed pattern. The rotational speed cannot evolve as quickly as before, losing part of the available power from the wind, as can be seen in Figure 20d. This fact proves that during the test, the turbine operates less time in the neighbourhood of the maximum Cp, producing less energy.

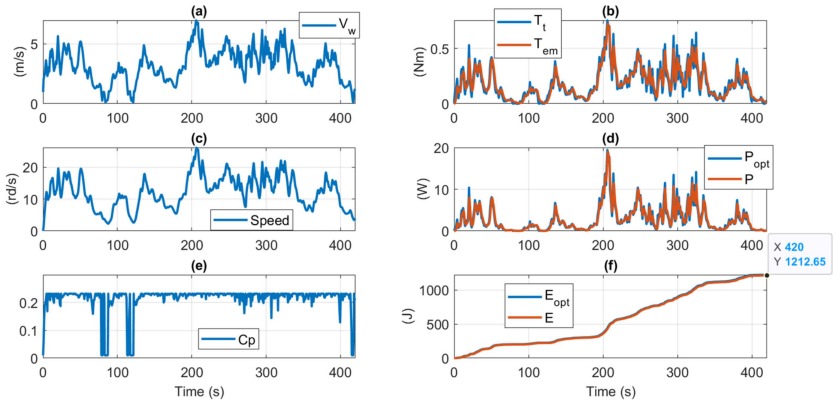

Figure 19. Performance of the Ayanz Wind Turbine based on Screw Blades with idealised Indirect MPPT control and inertia of J = 0.03 kgm^2. (**a**) Wind speed pattern, (**b**) Tt and Tem performances, (**c**) achieved rotational speed by the idealised MPPT control, (**d**) Optimal power with a fictitious turbine with zero inertia (Popt) and actual power generated, (**e**) Behaviour of Cp during the test, (**f**) energy generated at the 420 s test.

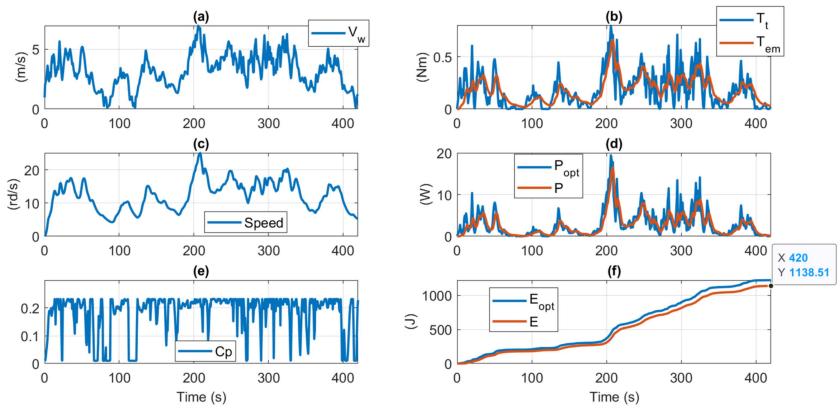

Figure 20. Performance of the Ayanz Wind Turbine based on Screw Blades with idealised Indirect MPPT control and inertia of J = 0.15 kgm^2. (**a**) Wind speed pattern, (**b**) Tt and Tem performances, (**c**) achieved rotational speed by the idealised MPPT control, (**d**) Optimal power with a fictitious turbine with zero inertia (Popt) and actual power generated, (**e**) Behavior of Cp during the test, (**f**) energy generated at the 420 s test.

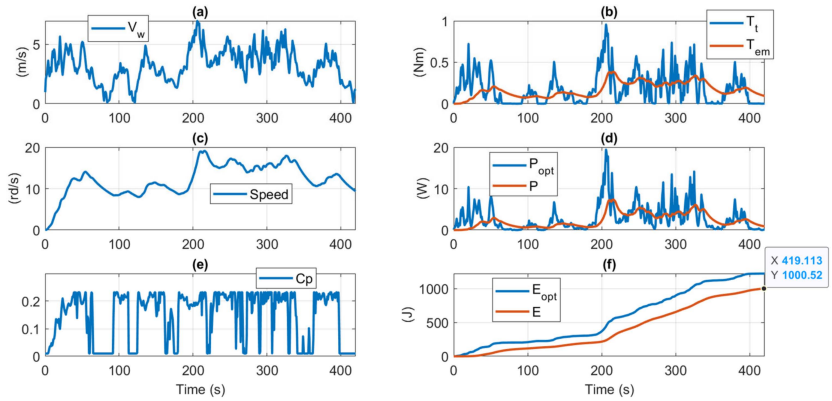

Figure 21. Performance of the Ayanz Wind Turbine based on Screw Blades with idealised Indirect MPPT control and inertia of J = 0.75 kgm^2. (**a**) Wind speed pattern, (**b**) Tt and Tem performances, (**c**) achieved rotational speed by the idealised MPPT control, (**d**) Optimal power with a fictitious turbine with zero inertia (Popt) and actual power generated, (**e**) Behaviour of Cp during the test, (**f**) energy generated at the 420 s test.

Then, in the third experiment shown in Figure 21 with an inertia of J = 0.75 kgm^2, which is again 5 times bigger than the previous case, the idealised MPPT still produces less energy since the bigger inertia does not enable the wind turbine to follow the required rotational speed for maximising energy. As summarised in Table 2, in the second experiment, 94% of the achievable energy was obtained, while in the third experiment, the energy obtained was further reduced up to 82.5%.

Table 2. Energy is generated with a wind speed pattern of 420 s, the same ideal wind turbine and the same wind speed patterns at different inertia.

Energy Generated During the Ideal Wind Turbine Test		
Inertia	**Energy**	**% of Energy**
J = 0.03 kgm^2	1212.65 J	100%
J = 0.15 kgm^2	1138.52 J	94%
J = 0.75 kgm^2	1000.52 J	82.5%

This tendency clearly demonstrates that the inertia of the wind turbine is a key parameter when designing small wind turbines to be placed in urban areas of city locations, where the wind speed varies quite quickly. Therefore, if the generated energy wants to be maximised, wind turbine morphologies whose equivalent inertias are 'small' are more suitable to be used. If it is possible, light materials that further minimise the inertia of the blades would be the best option, but as always, finding equilibrium with mechanical robustness is the best.

After these six minutes of performance analysis, the same study is applied to a longer period of time and at different types of wind days. By using the same time domain simulation programs as before, equal comparison performance is carried out, employing 8 h of wind measurements of low wind, moderate wind and extremely high wind days (Figures 14–16 partially show these wind measurements). The wind measurements are taken with a sample time of 1 s, while the simulation runs at 0.01 s sample time (Figure 18). As depicted in Table 3, it is noticed here again that the bigger inertia produces a reduction of the energy extracted from the wind turbine blades from the wind, no matter how the wind is. At these types of city locations, the wind is gusty and continuously varies, so low inertia facilitates tracking the rotational speed required to follow the MPPT power values. Then, from the results, it can also be concluded that very windy days work more time at MPPT effective points than lower wind days because the rotational speed and torque values of operation are further away from the zero-speed value. This means that on extremely windy days, the wind turbines are rotating more time, avoiding zero speed of operation and, therefore, avoiding the inefficient start-up processes of the wind turbine.

Finally, in the long-term energy production analysis, Table 4 shows the one-year energy production estimation and capacity factor estimations of this specific wind turbine. The energy production estimation is calculated as defined by the Standard IEC 61400 [34] by using a Rayleigh distribution function (Weibull distribution with k = 2) and considering the averaged wind speed of the site of 1.2 m/s. Then, for comparison purposes with the previous analysis summarised in Table 3, the energy production estimation of 8 h is also provided in Table 4. Regarding the capacity factor estimations, it is noticed that by selecting the rated power of the wind turbine closer to the range of averaged power provided by the wind turbine at the site, the capacity factor is bigger. It is also seen that if the winds are bigger, the energy production of the wind turbine is also bigger, and therefore, the capacity factor indicators are bigger as well. Finally, it is seen that the energy production estimation in 8 h, according to the IEC 61400, is slightly different from the energy estimation calculated by the time domain simulations that consider the dynamic responses associated with the inertia. To conclude, from now on and hereafter, the analysis will focus on the 6 min time domain simulations, focusing on the short-term periods of time, for simplicity.

Table 3. Energy is generated at 3 different wind days with the same ideal wind turbine at different inertia (The energy is calculated with time domain simulations, with real wind measurements at 1 s sample time).

	Low Inertia (J = 0.03 kgm^2)	**Normal Inertia (J = 0.15 kgm^2)**	**High Inertia (J = 0.75 kgm^2)**
Energy generated at a low wind day (8 h of day 4th October, Vav = 0.21 m/s, Vpeak = 2.3 m/s)	273 J	248 J	224 J
% of available energy with this specific wind turbine	93% (available: 293.5 J)	84.6% (available: 293.5 J)	76.4% (available: 293.5 J)
Energy generated at a moderate wind day (8 h of day 15th October, Vav = 0.7 m/s, Vpeak = 8.5 m/s)	5420 J	4813 J	4096 J
% of available energy with this specific wind turbine	96% (available: 5647 J)	85.2% (available: 5647 J)	72.5% (available: 5647 J)
Energy generated at a strong wind day (8 h of day 9th October, Vav = 3.5 m/s, Vpeak = 21 m/s)	279 kJ	268.29 kJ	246.54 kJ
% of available energy with this specific wind turbine	99.9% (available: 279 kJ)	96.2% (available: 279 kJ)	88.5% (available: 279 kJ)

Table 4. Energy and Capacity Factor estimations as defined by the Standard IEC 61400 [34] in two different periods of time, with wind speed measurements of the site and wind measurements corrected by factor 1.4 in order to estimate the wind at a location 4 m higher. Capacity Factor = Energy/(TimexPrated).

	Energy	**Capacity Factor (Prated = 20 W)**	**Capacity Factor (Prated = 4 W)**	**Energy**	**Capacity Factor (Prated = 20 W)**	**Capacity Factor (Prated = 4 W)**
	Measured Wind			**Measured Wind Corrected by 1.4 Factor at 4 m Higher Height**		
Energy and Capacity Factor estimation with Rayleigh distribution in one year (as defined the Standard 61400 [34]: 365 days with Vav = 1.2 m/s)	6613 kJ	1%	5.2%	17,062 kJ	2.7%	13.5%
Energy and Capacity Factor estimation with Rayleigh distribution in 8 h (as defined the Standard 61400 [34]: 8 h with Vav = 1.2 m/s)	6 kJ	1%	5.2%	16 kJ	2.7%	13.5%

4.3. Performance Analysis with Different MPPT Control Dynamics

In this sub-section, the effect of the closed-loop control dynamics of the MPPT on the energy production of the wind turbine is analysed. In this case, the employed wind turbine model incorporates the PM generator, the rectifier and the DC-DC converter, together with a realistic MPPT control, as presented in Figure 22. The entire model has been implemented in Matlab-Simulink, as can be noticed, compared with the block diagram presented in Figure 4 of the previous section, a low pass filter has been included at the input of the current reference i_{dc}. This is necessary to guarantee the stability of the closed-loop system performance. Note that the oscillations or ripples that could present V_{dc1}, if they are not filtered, can be feedbacked to the current loop, increasing them over and over again to V_{dc1} until stability is lost. In order to avoid this undesired situation, a typical and easy solution is to include a low pass filter, as illustrated in Figure 22. The value for the time constant τ, in general, is simply tuned by trial and error since it depends on the electric parameters characteristics as well as the tendency to produce torque and speed oscillations of the specific morphology of the wind turbine studied. Other filters or smoothing philosophies could be adopted, but in this case, for simplicity, a simple first-order filter has been used.

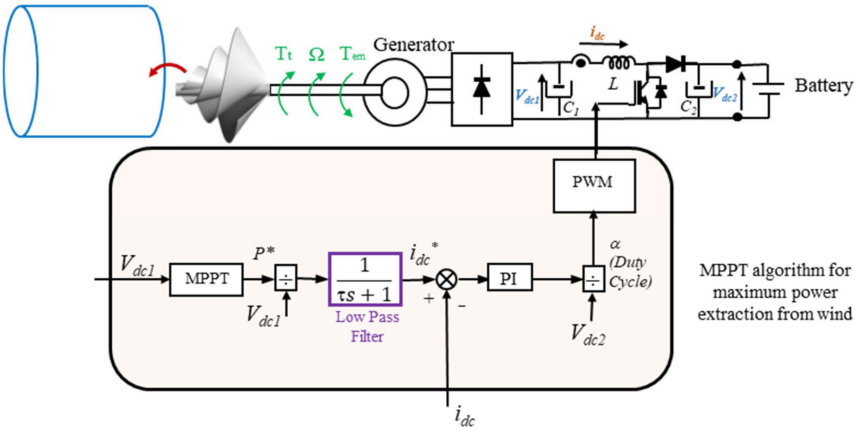

Figure 22. Indirect Speed Control MPPT that includes a low pass filter to ensure the stability of the system.

Hence, Figures 23 and 24 show the performance of the Ayanz Wind Turbine with Screw Blades with Indirect MPPT control and different time constants (τ) of low pass filter for smoothing V_{dc1} oscillations. In this case, a realistic value of J = 0.15 kgm^2 inertia has been adopted.

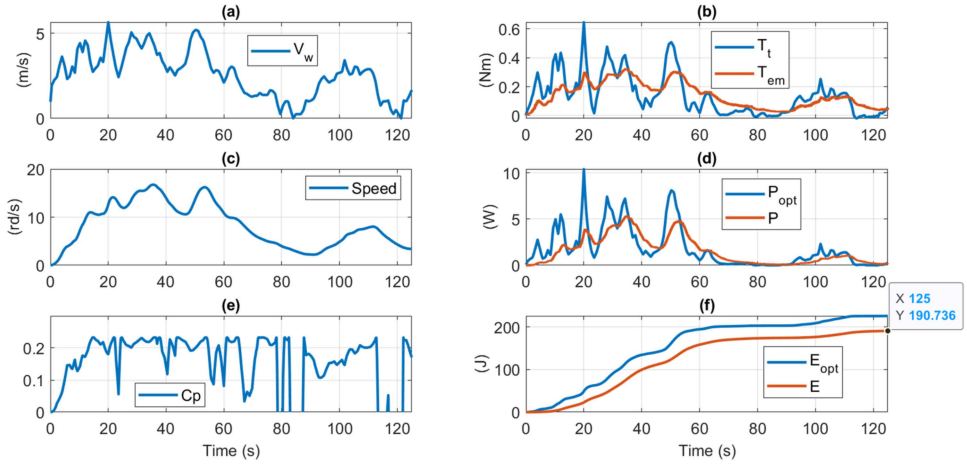

Figure 23. Performance of the Ayanz Wind Turbine based on Screw Blades with Indirect MPPT control and τ = 1 s at low pass filter for smoothing V_{dc1} oscillations (J = 0.15 kgm^2, $V_{battery}$ = 48 V). (**a**) Wind speed pattern, (**b**) Tt and Tem performances, (**c**) achieved rotational speed by the idealised MPPT control, (**d**) Optimal power with a fictitious turbine with zero inertia (Popt) and actual power generated, (**e**) Behavior of Cp during the test, (**f**) energy generated at the 125 s test.

The wind speed pattern is the first 125 s of the previously employed wind speed pattern. In Figure 23, with a realistic τ = 1 s, it is seen that the energy generated at the mechanical shaft of the generator (190.7 J) is below the maximum available energy at each wind speed. This happens due to the filter-introduced delay, the generator's dynamic delay and the inertia delay itself. However, when the quite extreme unfavourable case of τ = 6 s is tested, as depicted in Figure 24, the achieved energy is further reduced to 185 J (3%). This means that the closed-loop control dynamic, mainly determined by this filter dynamic (because the generator's electric dynamic and the current loop dynamics are normally faster), can also slow down the turbine's performance, moving away from the maximum values of Cp and therefore, further reducing the generated energy.

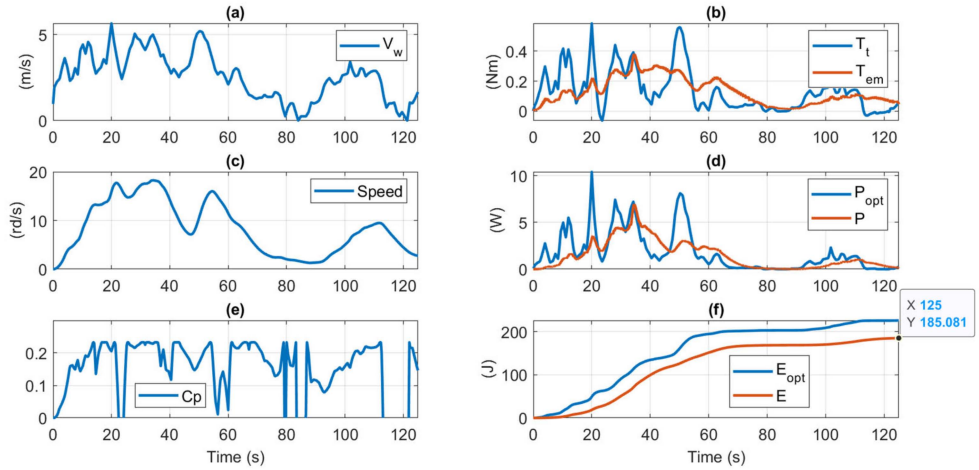

Figure 24. Performance of the Ayanz Wind Turbine based on Screw Blades with Indirect MPPT control and τ = 6 s at low pass filter for smoothing V_{dc1} oscillations (J = 0.15 kgm^2, $V_{battery}$ = 48 V). (**a**) Wind speed pattern, (**b**) Tt and Tem performances, (**c**) achieved rotational speed by the idealised MPPT control, (**d**) Optimal power with a fictitious turbine with zero inertia (Popt) and actual power generated, (**e**) Behavior of Cp during the test, (**f**) energy generated at the 125 s test.

4.4. Performance Analysis with Uncertainty at MPPT Curve

In this sub-section, the uncertainty of the MPPT curve is analysed in the energy production of the wind turbine. In this case, the same wind turbine model is employed as in the previous sub-section, but an additional realistic fact has been considered at the control. Often, the MPPT curve P = f(V_{dc1}) is not so accurately known due to many reasons. Perhaps the principal one is the fact that often the wind turbine cannot be accurately characterised (there is no availability of wind tunnel to excite the turbine as desired, accurate wind sensors are not available, electric power sensors are not available, etc.). Knowing this, it is not realistic to study the performance of the wind turbine assuming that an exact P = f(V_{dc1}) is known, which is a very common situation in many commercial wind turbines. In addition, these scenarios often operate at low-cost conditions, using not-so-accurate current or voltage sensors for the MPPT algorithm. Hence, considering all that is said here, the MPPT control considering uncertainties has been implemented in Matlab–Simulink, as depicted in Figure 25.

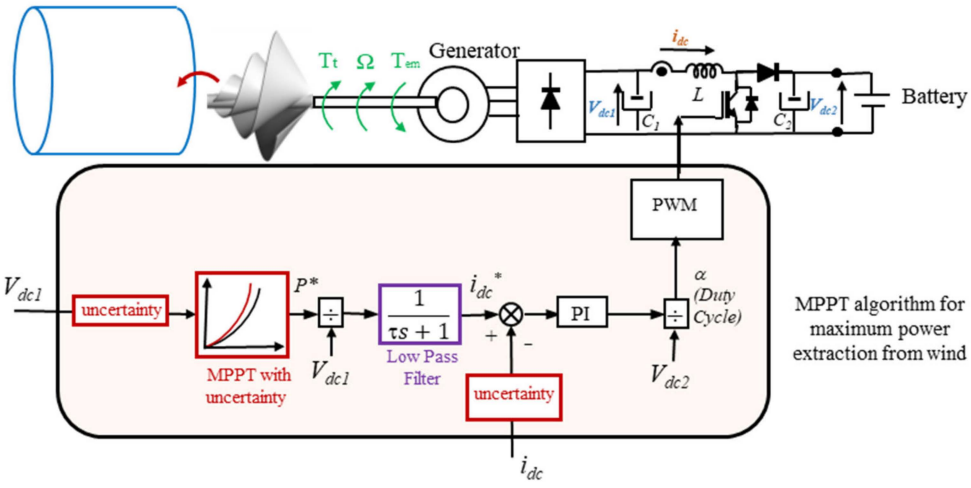

Figure 25. Indirect Speed Control MPPT includes a low pass filter to ensure the stability of the system and also uncertainties at the MPPT curve and current and voltage sensors.

As before carried out experiments, the low pass filter has also been left at the MPPT control algorithm while the inertia is also left to the realistic case of J = 0.15 kgm^2. Hence, an

equivalent simulation model-based test has been performed as in the previous sub-section, with the same wind speed pattern but, in this case, with a realistic uncertainty at the MPPT curve of 20% (optimum constant k with an error of 20%) and error at the current and voltage sensors of 5%. The results of the experiments are shown in Figure 26. Compared with the results of the previous sub-section of Figure 23, it is seen that the realistic uncertainty provokes a further reduction of the generated energy from 190.7 J to 182.1 J (around 5% reduction in 125 s of the test). This important fact is not often studied but is present in many small wind turbine designs.

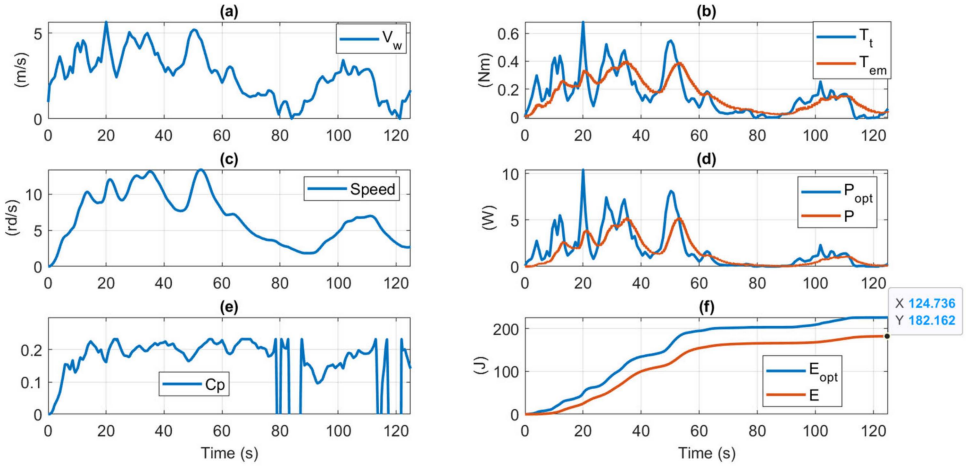

Figure 26. Performance of the Ayanz Wind Turbine based on Screw Blades with Indirect MPPT control and uncertainty at the MPPT curve of 20% (optimum constant k with an error of 20%) and error at the current and voltage sensors of 5% (τ = 1 s at low pass filter, J = 0.15 kgm^2, $V_{battery}$ = 48 V). (**a**) Wind speed pattern, (**b**) Tt and Tem performances, (**c**) achieved rotational speed by the idealised MPPT control, (**d**) Optimal power with a fictitious turbine with zero inertia (Popt) and actual power generated, (**e**) Behavior of Cp during the test, (**f**) energy generated at the 125 s test.

4.5. Performance Analysis of Pseudo-MPPT and Only Rectifier Power Conversion Systems

In this sub-section, the other two simplified power conversion topologies are analysed. In both cases, the same electric generator, rectifier, and C1 capacitance were used as in previous subsections when MPPT control was implemented. Hence, first of all, Figure 27 shows the only-rectifier performance with the same wind speed pattern as previous tests. A battery of 36 V was used after testing battery voltages of 12 V, 24 V, and 48 V, and the results were worse than those of 36 V at this wind pattern. It is seen that an energy of 178.36 J is obtained in this case, which is very close to the previous experiment with MPPT (only 2% energy reduction).

Obviously, in this case, the rotational speed is maintained quite constant, and the variations are due to the voltage droop at the parasitic resistance and inductances of the generator (Rs = 9.56 Ω, Ls = 20.96 mH). Thus, it is observed that at this wind speed pattern, by choosing a 36 V battery, it is possible to obtain quite good energy generation results. Then, in Figure 28, the same experiment is carried out, but now it includes an external inductance of L = 30 mH in order to perform a pseudo-MPPT. It is seen that the achieved generated energy is slightly smaller than in the previous experiment without external L. After several trials, it has been seen that the only way of increasing the energy generated would be, in this situation, by reducing the total L of the generator. As depicted in Figure 29, with the Only-Rectifier power conversion systems and a reduction of the parasitic Ls inductance of Ls = 20.96/3 mH, the generated energy of the system is increased to 189 J, which is a 4% energy increase with respect to the MPPT power conversion system (Figure 26).

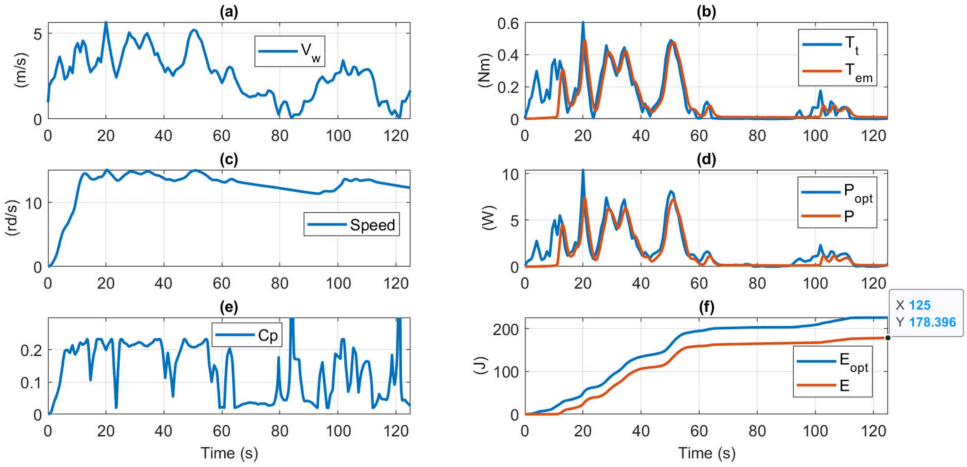

Figure 27. Performance of the Ayanz Wind Turbine based on Screw Blades with Only-rectifier power conversion system (J = 0.15 kgm^2, $V_{battery}$ = 36 V). (**a**) Wind speed pattern, (**b**) Tt and Tem performances, (**c**) achieved rotational speed by the idealised MPPT control, (**d**) Optimal power with a fictitious turbine with zero inertia (Popt) and actual power generated, (**e**) Behaviour of Cp during the test, (**f**) energy generated at the 125 s test.

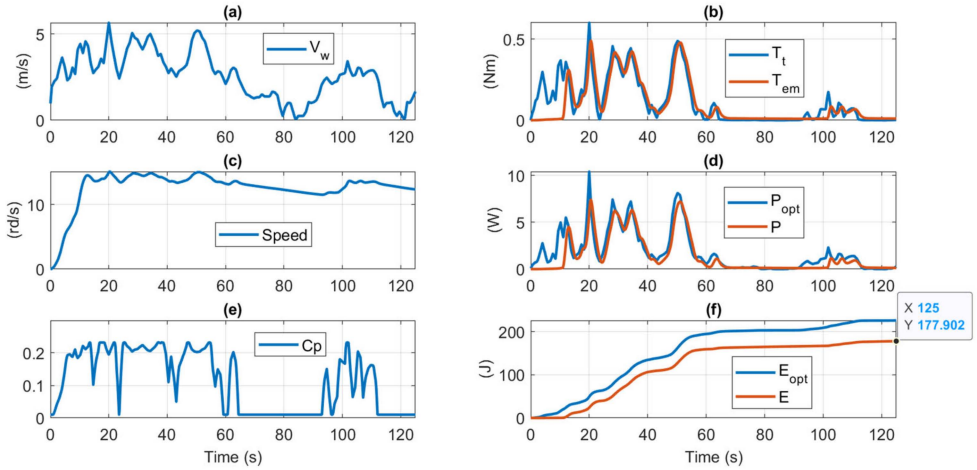

Figure 28. Performance of the Ayanz Wind Turbine based on Screw Blades with pseudo-MPPT power conversion system and external L = 30 mH (J = 0.15 kgm^2, $V_{battery}$ = 36 V). (**a**) Wind speed pattern, (**b**) Tt and Tem performances, (**c**) achieved rotational speed by the idealised MPPT control, (**d**) Optimal power with a fictitious turbine with zero inertia (Popt) and actual power generated, (**e**) Behavior of Cp during the test, (**f**) energy generated at the 125 s test.

In a real case, it would represent a change in the generator with a had-oc design, trying to reduce the parasitic inductance whenever possible and practical to be achieved. It has to be highlighted that the only-rectifier and pseudo-MPPT conversion systems will have fewer electric losses due to the omission of the DC-DC converter and the microprocessor, which could range around 1.5 W using standard electric components. Note that in all the cases, the power and energy that are being evaluated are at the mechanical shaft of the turbine. In addition, the MPPT system, as a drawback compared with the other two simpler versions, needs to tune control parameters and quite accurately know the turbine aerodynamic performance (k constant).

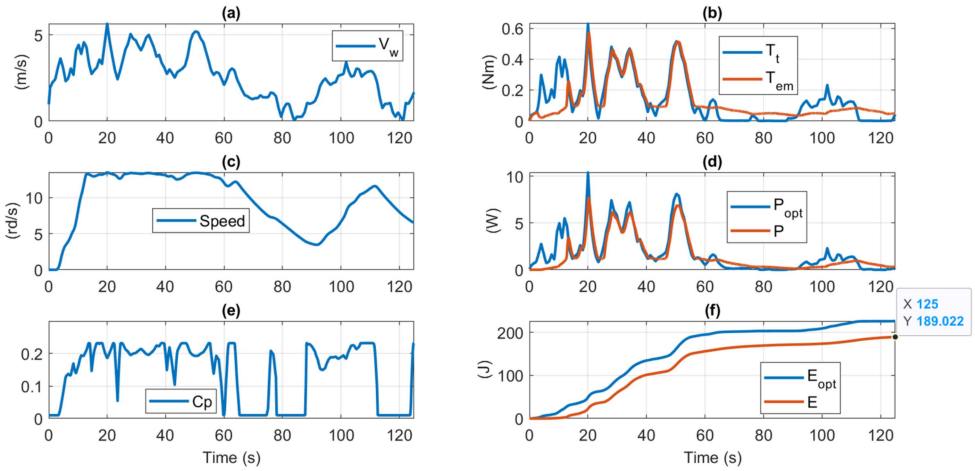

Figure 29. Performance of the Ayanz Wind Turbine based on Screw Blades with Only-rectifier power conversion system and generator's inductance of Ls divided by 3 (J = 0.15 kgm^2, $V_{battery}$ = 36 V). (**a**) Wind speed pattern, (**b**) Tt and Tem performances, (**c**) achieved rotational speed by the idealised MPPT control, (**d**) Optimal power with a fictitious turbine with zero inertia (Popt) and actual power generated, (**e**) Behavior of Cp during the test, (**f**) energy generated at the 125 s test.

4.6. Performance Analysis of a Wind Turbine with a Shorter Range of Values with Cpmax (Peaked Cp Curve)

In this last sub-section, the previously analysed power conversion configurations are tested in a fictitious wind turbine with a shorter range of values with Cpmax. Thus, as depicted in Figure 30, the new turbine to be studied presents a thinner range of lambda values where the Cp values are close to the Cpmax. This, again, a possible and realistic situation depending on the morphology of the wind turbine, will require a more precise and quicker MPPT control to operate at Cpmax values since a short rotational speed deviation from the optimum will imply a higher loss of efficiency than the previously studied wind turbine.

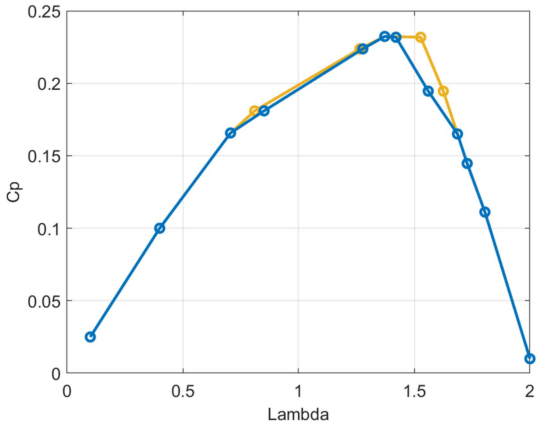

Figure 30. Cp(λ) curve of the Ayanz Wind Turbine based on Screw Blades used for the second set of simulations analyses (Blue: new Cp curve, Yellow: previous tests' Cp curve) with a shorter range of values with Cpmax.

Hence, Figures 31–33 present the same tests as performed in previous subsections, with the same wind patterns of 125 s of duration and with the three proposed power conversion systems. In Figure 31, it can be noticed that with this more peaked Cp(λ) curve, the Indirect MPPT generates less energy (178.5 J) than with the previous Cp curve (182.1 J in Figure 26).

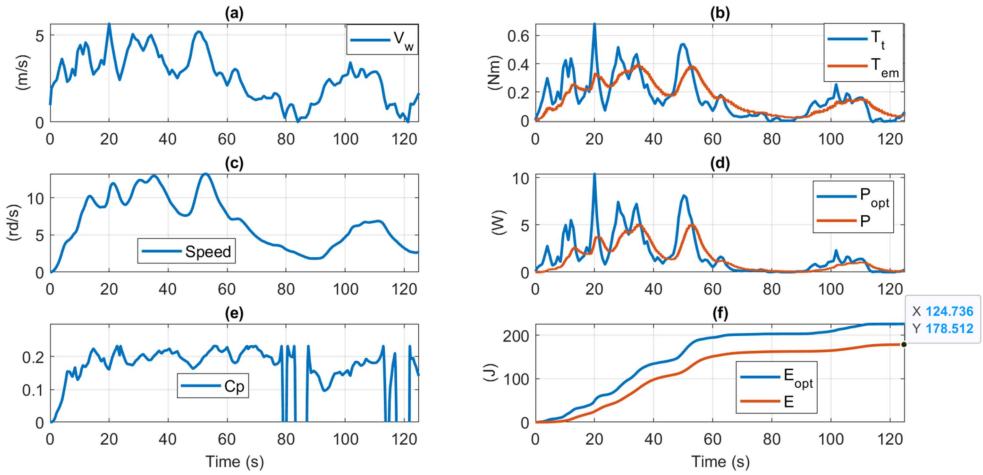

Figure 31. Performance of the Ayanz Wind Turbine based on Screw Blades with Indirect MPPT control and second more peaked curve of Cp = f(λ) (uncertainty at the MPPT curve of 20%, error at the current and voltage sensors of 5%, τ = 1 s at low pass filter, J = 0.15 kgm^2, $V_{battery}$ = 48 V). (**a**) Wind speed pattern, (**b**) Tt and Tem performances, (**c**) achieved rotational speed by the idealised MPPT control, (**d**) Optimal power with a fictitious turbine with zero inertia (Popt) and actual power generated, (**e**) Behavior of Cp during the test, (**f**) energy generated at the 125 s test.

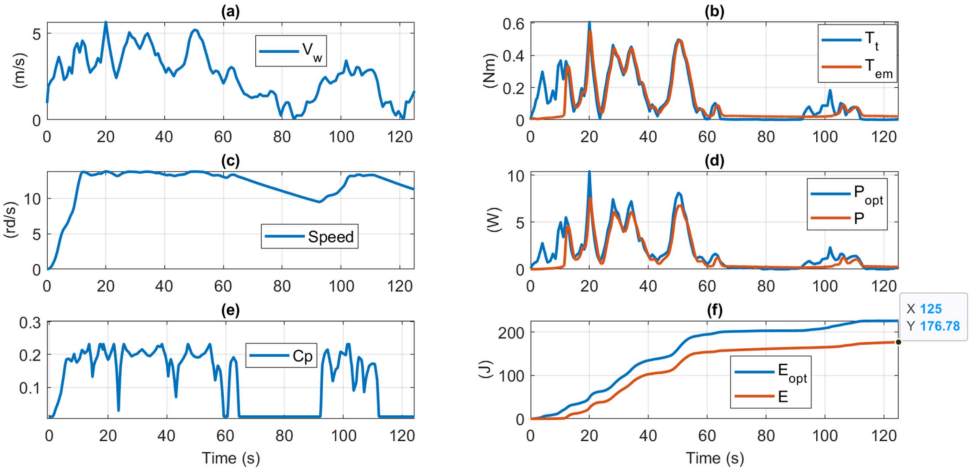

Figure 32. Performance of the Ayanz Wind Turbine based on Screw Blades with Only-Rectifier power conversion system and second more peaked curve of Cp = f(λ) (J = 0.15 kgm^2, $V_{battery}$ = 36 V). (**a**) Wind speed pattern, (**b**) Tt and Tem performances, (**c**) achieved rotational speed by the idealized MPPT control, (**d**) Optimal power with a fictitious turbine with zero inertia (Popt) and actual power generated, (**e**) Behavior of Cp during the test, (**f**) energy generated at the 125 s test.

As commented before, this is due to the fact that the MPPT control, accompanied by its uncertainties and delays in responses, is not able to avoid a certain deviation from the optimum rotational speed that finally generates a bigger deviation from the Cp maximum value. The difference is nearly 2%, which is not so high but gives an idea of how the characteristics of the wind turbine, combined with the control parametrisation and the wind patterns, can produce certain energy variations.

Then, in Figure 32, the performance of the Ayanz Wind Turbine based on Screw Blades with an Only-Rectifier power conversion system and a second more peaked curve of Cp = f(λ) is shown. Again, there are not big differences, and the generated energy is around 176.8 J, compared with the previous wind turbine (178.4 J in Figure 30).

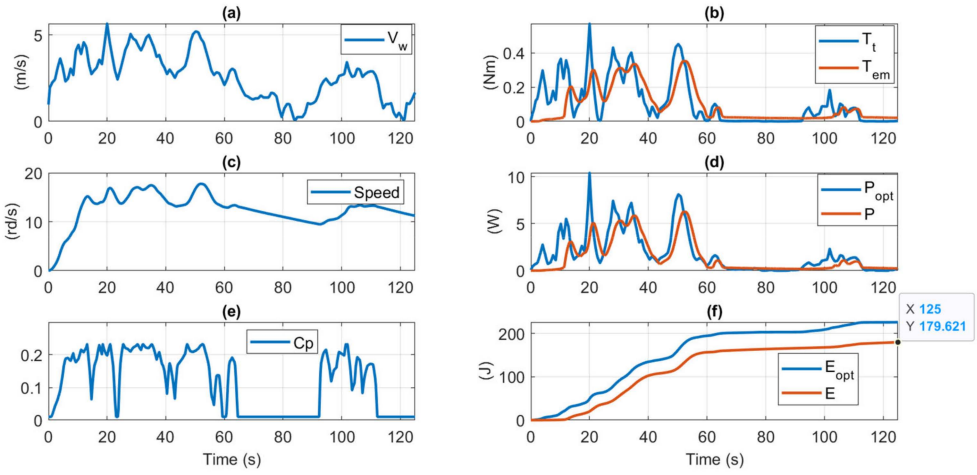

Figure 33. Performance of the Ayanz Wind Turbine based on Screw Blades with pseudo-MPPT power conversion system (series external C = 0.1 mF at three phases) and second more peaked curve of Cp = f(λ) (J = 0.15 kgm^2, $V_{battery}$ = 36 V). (**a**) Wind speed pattern, (**b**) Tt and Tem performances, (**c**) achieved rotational speed by the idealized MPPT control, (**d**) Optimal power with a fictitious turbine with zero inertia (Popt) and actual power generated, (**e**) Behaviour of Cp during the test, (**f**) energy generated at the 125 s test.

Finally, several simulations have been carried out using the pseudo-MPPT concept with this more peaked Cp wind turbine. It has been noticed that with external inductances, it has not been possible to improve the generated energy. However, it has been observed that by including series capacitive impedances, the improvement has been possible. Thus, Figure 33 shows the pseudo-MPPT power conversion system with series external C = 0.1 mF at the three phases and a second more peaked curve of Cp = f(λ). It can be observed that the generated energy now is 179.6 J, which is the highest obtained energy with this more peaked Cp curve. Again, the differences are not significant, but they give the idea that the MPPT is not always the best option for maximising the generated energy. Wind speed conditions, together with key characteristics of the wind turbine (inertia, shape of the Cp curve), can provoke that any of the three studied power conversion configurations could be the one that maximises the generated power. Consequently, it is often possible that we can avoid the utilisation of complex MPPT controls and go for simpler, cheaper, and less power loss configurations such as the pseudo-MPPT or even the Only-Rectifier version.

Finally, Table 5 summarises the last results obtained from this simulation-based analysis, together with a few others not shown previously. It is seen that for both Cp curves of two possible specific wind turbines (peaked and non-peaked), the Only-Rectifier power conversion system can achieve almost the same energy generation as a realistic MPPT power conversion (from 182.1 J to 178.3 J ⇒ 2.1% and from 178.5 J to 176.8 J ⇒ 1%), being this difference almost unappreciable at the case of the Cp peaked curve wind turbine.

Then, with the pseudo-MPPT power conversion, the generated energy can be further improved in comparison to the Only-Rectifier configuration, obtaining closer or even better energy generation results than the MPPT if the impedance value is well chosen and also the Vbattery voltage. Thus, it is seen that with a reduced Ls impedance design of the generator, the energy generated with the first non-peaked Cp wind turbine can be improved from 182.1 J to 189 J (⇒3.8%). Finally, with the second Cp peaked curve, by including an external capacitance of 0.1 mF, the pseudo-MPPT improves to the MPPT from 178.5 J to 179.6 J (⇒0.6%). All these obtained results and behaviours are due to a combination of multiple factors: Inertia of the wind turbine, the shape of the Cp curve, electric parameters of the generator, voltage of the battery, control parameters and shape of the wind gusts or patterns.

Table 5. Summary of the results obtained at the comparison between power conversion system configurations.

	Energy Generated with First Cp(λ)	**Energy Generated with Second Cp(λ) (Peaked Curve)**
MPPT ($J = 0.15\ kgm^2$, uncertainty at MPPT curve: 20%, error at I and V sensors; 5%, $\tau = 1$ s at LP filter, $J = 0.15\ kgm^2$)	182.1 J	178.5 J
Only-Rectifier ($J = 0.15\ kgm^2$, $V_{battery} = 36$ V)	178.3 J	176.8 J
Pseudo-MPPT, including an external L = 30 mH ($J = 0.15\ kgm^2$, $V_{battery} = 36$ V)	177.9 J	176.1 J
Pseudo-MPPT, reducing the parasitic Ls of the generator by 3 ($J = 0.15\ kgm^2$, $V_{battery} = 36$ V)	189 J	175.3 J
Pseudo-MPPT, including external C = 0.1 mF ($J = 0.15\ kgm^2$, $V_{battery} = 36$ V)	177.6 J	179.6 J

4.7. Closure. Summary of the Simulation-Based Analysis

In this sub-section, a summary of the previously obtained simulation-based analysis is served. Table 6 covers the most important qualitative conclusions of the performed analysis. As can be noticed, in general, it can be concluded that wind turbines placed at gusty locations, with designs that minimise inertia, are the best positioned. Then, simple Only-rectifier and pseudo-MPPT power conversion configurations can obtain very similar energy production or even better than more complex and expensive MPPT systems.

Table 6. Summary of the results obtained at the simulation-based analysis.

	Conclusion
Affection of the Inertia of the Wind Turbine	- In Urban City locations, where the wind speed is gusty, wind turbines with smaller inertia are able to extract more energy from the wind. - This is due to the fact that the big inertias, do not allow to the wind turbine quickly reach the optimal variable rotation speeds, corresponding to the quick varying wind speeds.
MPPT Power Conversion System	- In Urban City locations, where the wind speed is gusty, the quicker and more accurately is tuned the MPPT control, bigger energy can extract from the wind. - Again, this is due to the fact that uncertainties and dynamic delays at the control, produce not reaching the optimal rotation speeds of the wind turbine, corresponding to the quick varying wind speeds. - Wind turbines with non-peaked Cp curve characteristics, are more suitable for producing more energy with MPPT in gusty wind speed environments.
Only-Rectifier and Pseudo-MPPT Power Conversion Systems	- In Urban City locations, where the wind speed is gusty, these two much simpler, more reliable and less costly power conversion configurations can obtain very close generated energies to the MPPT conversion system. - Less than 5% loss of energy for the Only-Rectifier configuration in comparison to the MPPT. - The pseudo-MPPT, including an appropriate impedance (L or C depending on the turbine characteristics) at the conversion system, can produce even better energy generation results than the MPPT, for some types of wind gusts patterns. - In Wind turbines that present peaked Cp curve characteristics, placed at gusty wind locations, the energy generated by the MPPT is penalized so pseudo-MPPT and Only-Rectifier configurations, become more competitive compared to MPPT.

Finally, in the situation where a wind turbine is already designed (blades and mechanical parts), but the appropriate power conversion configuration is necessary to be chosen, the method schematically represented in Figure 34 can assist in the selection. Therefore, in a site with known wind patterns, a schematic flowchart based on an energy calculation optimises the set of parameters for each power conversion configuration and evaluates the corresponding cost returns. With this conceptual method, the optimised electric parameters can be selected, and the most cost-effective power conversion configuration can be deduced.

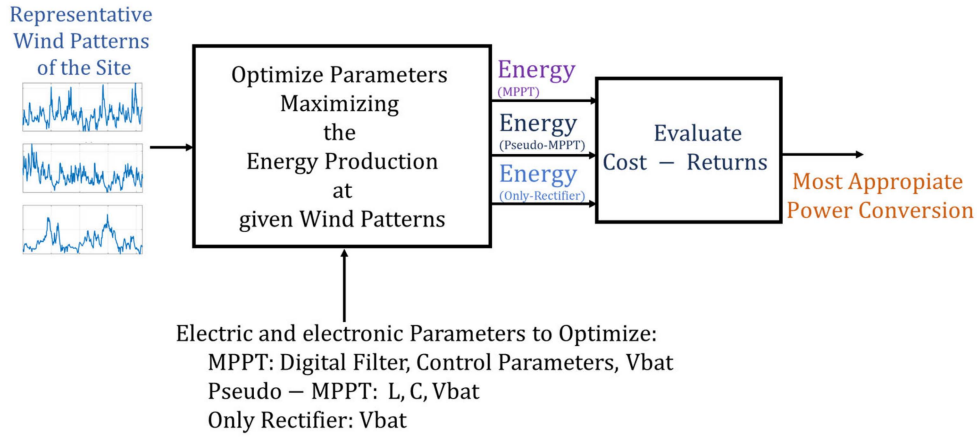

Figure 34. The flowchart shows the optimization-based method that can be applied to evaluate which electric power configuration is the most appropriate for a site with given representative wind patterns.

5. Experimental Test Results-Based Analysis

5.1. Wind Maker

In this subsection, an experimental-based analysis is carried out using a windmaker located at the power electronics laboratories of Mondragon University. The model of the wind maker is the VPA 1400SP of the manufacturer NLH Industrie (Jouars Pontchartrain, France) and is shown in Figure 35. This is a wind maker consisting of a single fan driven directly by a single 400 V, 50 Hz, 30 kW, four-pole induction motor [26]. This motor that moves the fan is controlled by a commercial ABB ACS550 electric drive (Zurich, Switzerland). At rated motor speed, an airflow of 100,000 m^3/hour is obtained. The motor speed is controlled by the electric drive and the airflow, and, therefore, the wind speed at the tunnel exit is controlled. Just behind the motor, the tunnel has a silencer, while at the outlet, it has a metal grid to uniform the airflow. The wind turbine to be tested is placed outside the tunnel at a fixed distance from it [26].

5.2. Real Wind Turbine Used at the Experimental Validation: The Ayanz Wind Turbine Based on Screw Blades

The wind turbine used in the experimental tests is the Ayanz Wind Turbine, based on Screw Blades previously shown in Figure 1. The aerodynamic characterisation of this commercially available turbine was published in a previous article, Ref. [26]. Since the wind maker produces a wind speed not equal to the whole area of the circumference outlet, in order to precisely know what wind is affecting the wind turbine, a mean of several wind measurements is carried out. An XA1000 Lufft portable wind speed sensor is placed at different input points of the turbine, which are marked in red in Figure 36a. For each point and frequency setpoint (wind speed setpoint), a measurement was taken in a time window of at least 25 s, and the velocities obtained during this interval were averaged. Figure 36b shows the results obtained and the averaged wind speed considered in blue, which is the mean of the red point measurements.

(**a**)

(**b**)

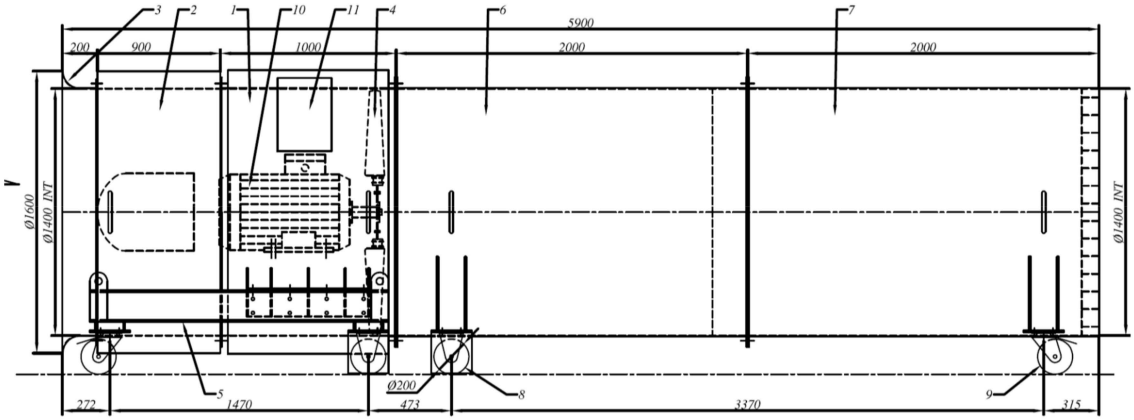

Figure 35. (**a**) Photo of the Wind maker used for the experimental validation at laboratories of Mondragon University, (**b**) characteristics of the wind maker [26].

(**a**)

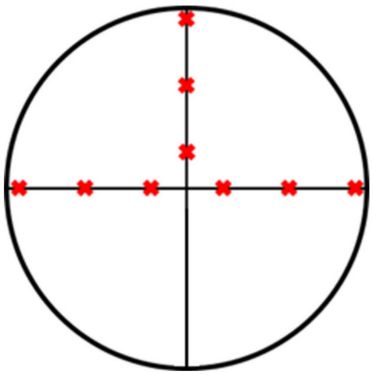

(**b**)

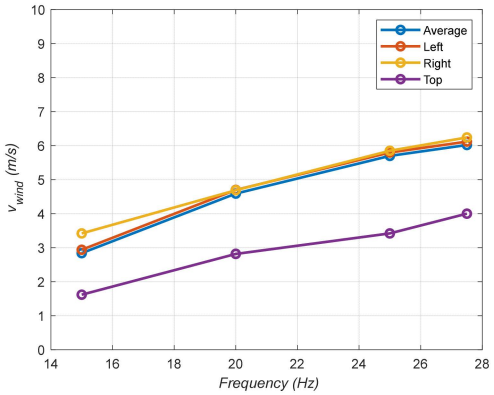

Figure 36. (**a**) Wind measurement points (in red) are taken just in the front area of the turbine, and (**b**) wind measurements are taken at the wind turbine's input with the tube (obtained and first published in [26]).

After that, once the wind speed measurements are obtained, experimental characterisation of the wind turbine is carried out. The wind turbine is excited with the wind maker, and the power at an external passive load located at the generators' output is measured. Then, the power curves of the wind turbine are obtained, as shown in Figure 37. For more information about the experimental characterisation, the reader is referred to [26].

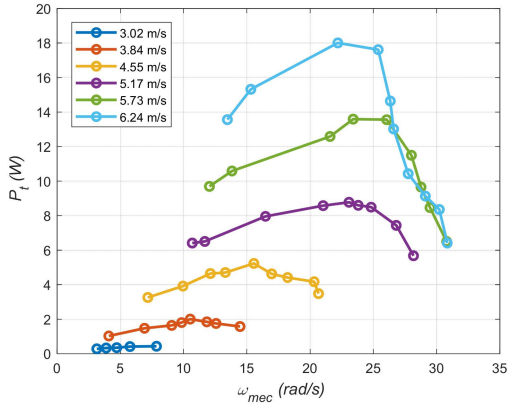

Figure 37. Power curves of the Ayanz Wind Turbine based on Screw Blades (obtained and first published in [26]).

Once the power curves of the wind turbine are characterised, Figure 38a,b shows the Power curves of the Ayanz Wind Turbine based on Screw Blades. First, in Figure 38a, curves with ideal MPPT and Only-Rectifier configurations at different battery voltages (24 V are 2 batteries in series while 40 V are 3 batteries in series) are shown, while in Figure 38b, ideal MPPT, only-Rectifier and pseudo-MPPT configurations at 40 V of battery voltage are provided. It has to be remarked that these curves are obtained with the wind maker producing a constant wind speed, which means that they are curves at steady-state operation conditions. However, as has been shown in the previous section, the wind at city locations is not constant since it varies in gusty shapes.

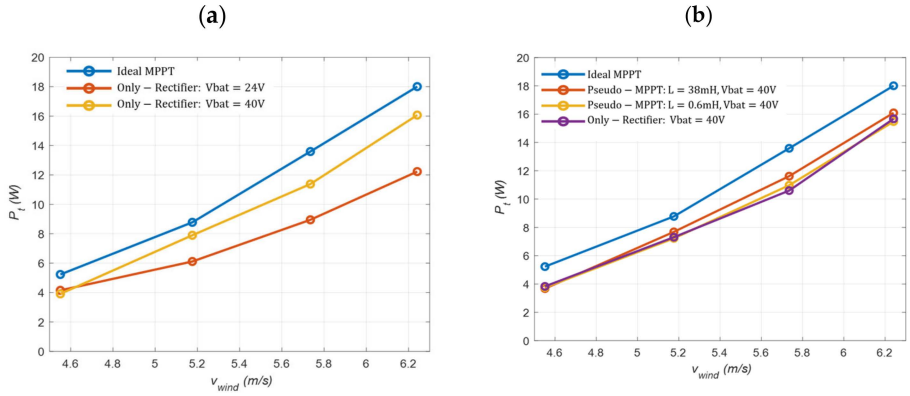

Figure 38. Power curves of the Ayanz Wind Turbine based on Screw Blades at constant wind speeds (obtained and first published in [26]). (**a**) Ideal MPPT and Only-Rectifier configurations at different battery voltages (24 V are 2 batteries in series while 40 V are 3 batteries in series). (**b**) Ideal MPPT, Only-Rectifier and pseudo-MPPT configurations at 40 V of battery voltage.

5.3. Wind Patterns Used at the Experimental Tests

Once the wind turbine is characterised, the next step is to test it at realistic variable wind speeds typical from city locations. In Figure 39, a graphical simplified pattern identification of wind speed measured in the urban area of Mondragon City is depicted. As noticed, the complex and very variable wind pattern can be somehow simplified to 'ramp-based' wind patterns superposed in the figure with red colour.

With the fastest variations of wind speed, wind turbines are not able to follow (at least with these dimensions) due to their natural intrinsic inertia. Therefore, during laboratory tests with the wind maker, the fastest wind variations will not be reproduced, and only 'ramp-based' wind speed variations will be implemented. In addition, it has to be highlighted that the wind maker does not have the capacity to reproduce very fast wind speed variations due to its dynamic response capacity limitation. So even if wanted, it would be

impossible to reproduce faithfully and accurately the quick varying wind speed pattern of Figure 39.

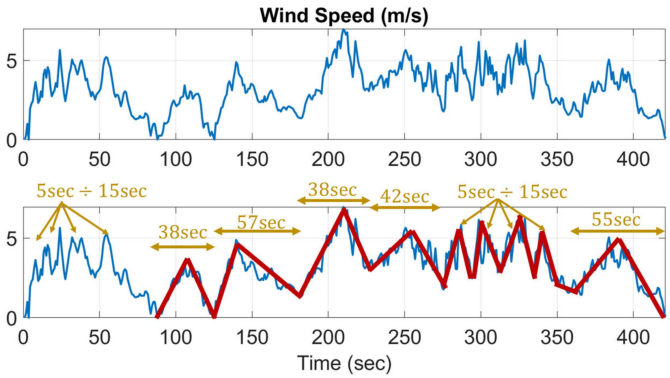

Figure 39. Simplified pattern identification of wind speed measured with XA1000 Lufft anemometer (sample time = 1 s) at a moderately windy day in Mondragon University in the urban area of the city (same wind pattern used in previous simulation-based analysis section).

Hence, Figure 40, in a simplified manner, shows that although, in reality, the typical pattern of wind gusts (neglected the fastest super-posed small wind variations) may present different increasing and decreasing slopes and different also starting and ending wind speeds, for simplicity, this fact will be neglected and equal initial-end slopes and winds will be considered, as depicted in Figure 40. Thanks to this simplification, the experimental validation is easier to perform. Otherwise, many wind patterns would need to be tested, with different increasing and decreasing slopes and different starting and ending points.

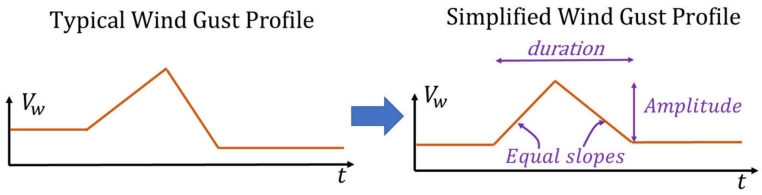

Figure 40. Simplified wind gust pattern used at laboratory tests in subsequent sections.

Consequently, the experimental test will be restricted to studying the behaviour of wind turbines to 'ramp-based' wind patterns and to measuring the power end energy generated by the wind turbine with different power conversion system configurations, as graphically illustrated in Figure 41. With this chosen pattern, a representative enough wind profile is tested, which is sufficient to corroborate with experimental results, as well as the general behaviours and tendencies obtained with simulation results in previous sections.

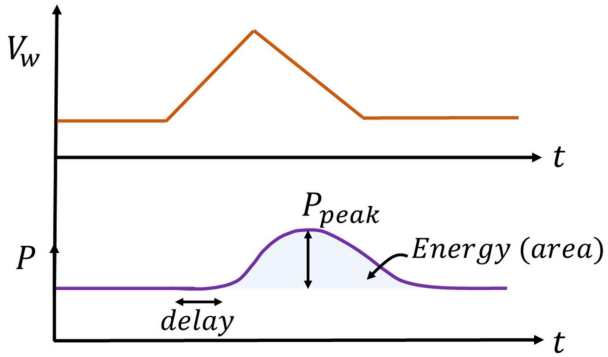

Figure 41. Simplified wind gust pattern used for the experimental tests, and power and energy obtained with the wind turbine.

5.4. Performance at Variable Wind Speed: Simplified 'Ramp-Based' Wind Gust Patterns

With the real wind patterns determined, the next step is to test their performance with the real Ayanz wind turbine and the only rectifier, the pseudo-MPPT and the MPPT. Each of these topologies is tested in four different scenarios, specifically, to four different wind gusts. Matlab's Simulink blocks were used to reproduce the 'ramp-based' wind gust patterns, and the four wind gust patterns were 20 s, 40 s, 60 s, and 80 s.

Likewise, the gusts are symmetrical, which means that half of the gust ascends to the maximum, and the other half descends from the maximum to the minimum. It is important to mention that during all the tests, the minimum and the maximum wind values have not been changed; the only ones changed have been the gust times. In order for the test to be the most accurate, the maximum and minimum values have been defined, taking into account all the data mentioned in Section 5.3, with the minimum wind reference of 3.51 m/s and the maximum wind reference of 5.73 m/s. It is important to mention that for all the tests developed during this section, the Ayanz was already spinning at 3.51 m/s. Hence, as depicted in Figure 42, the first analysed case has been the one related to the only rectifier. In all four cases, it can be seen that the power peak is given after the reference wind speed peak happens, meaning that a delay happens between both. This means that, in reality, the system behaves as it should (compared to Figure 41). Another important factor that can be seen is that the voltage on the batteries is lower than the voltage on the rectified side; this happens mainly due to the voltage drops that occur through the diodes of the converter.

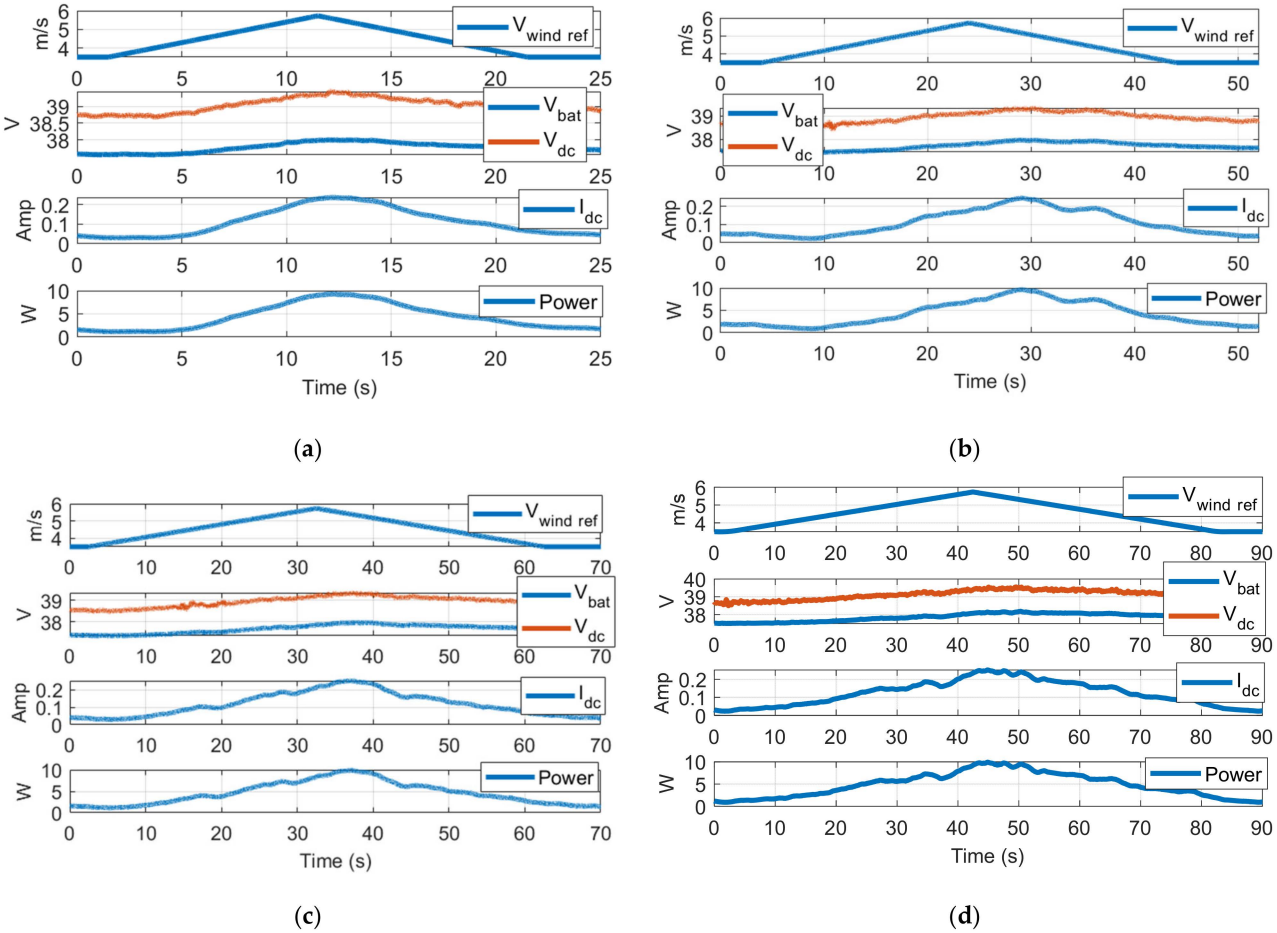

Figure 42. Performance of the Ayanz Wind Turbine with screw blades at variable wind speed tests, with only rectifier power conversion system. (**a**) 10 s + 10 s wind gust, (**b**) 20 s + 20 s wind gust, (**c**) 30 s + 30 s wind gust, (**d**) 40 s + 40 s wind gust.

Then, the results presented in Figure 43 are the ones related to the pseudo-MPPT. The inductance used for this has been 38 mH and has been placed before the rectifier in the three phases. As in the previous case, a delay appears between the wind reference maximum point and the peak power point, indicating positive results.

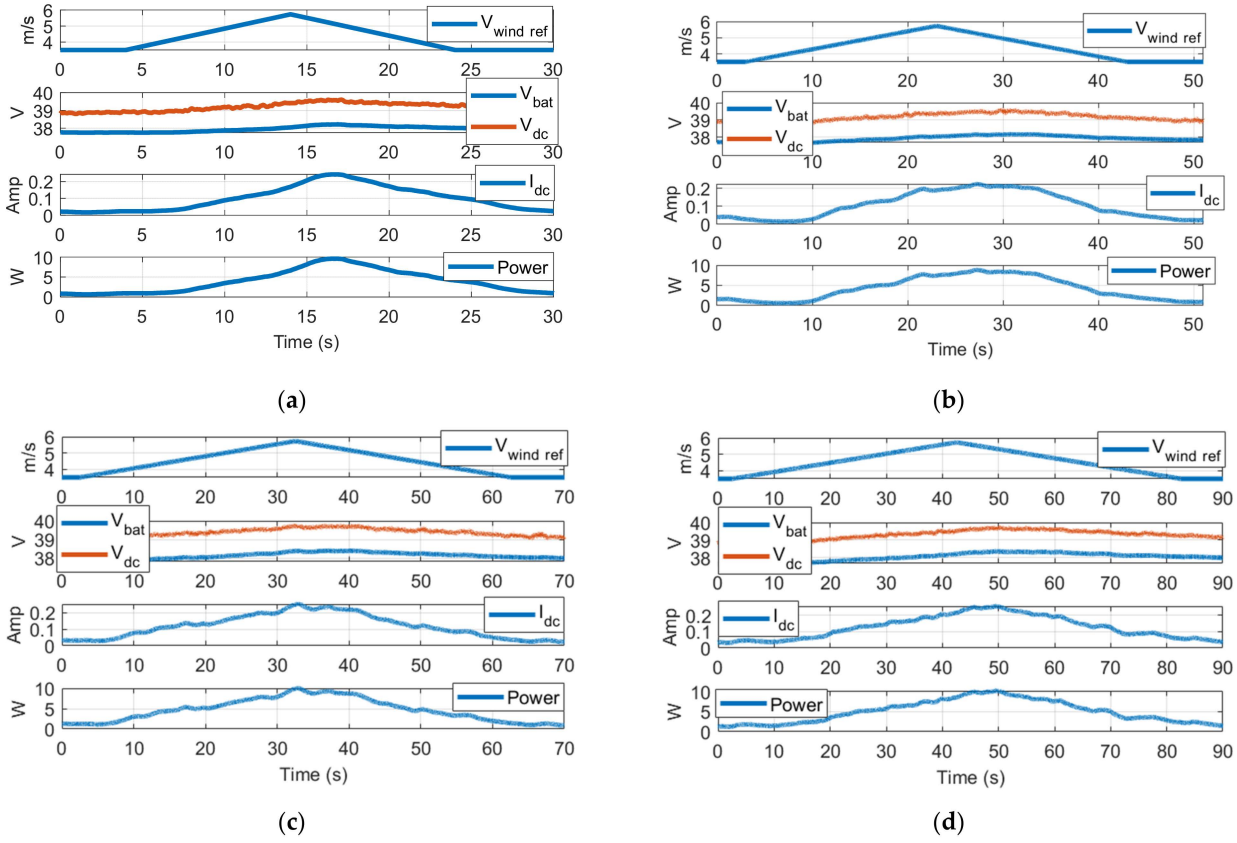

Figure 43. Performance of the Ayanz Wind Turbine with screw blades at variable wind speed tests, with pseudo-MPPT power conversion system with L = 38 mH. (**a**) 10 s + 10 s wind gust, (**b**) 20 s + 20 s wind gust, (**c**) 30 s + 30 s wind gust, (**d**) 40 s + 40 s wind gust.

Figure 44 shows the results related to the MPPT. In this case, it can be seen that Vdc1 is no longer constant and varies throughout the gust. This happens due to the MPPT system, which works based on the voltage that is measured and produces the power reference, affecting all the controlled systems. As in the previous two cases, the mentioned delay appears, proving the favourable results. Moreover, for the MPPT case, there is another important parameter that appears in the figure, i.e., the duty cycle. The behaviour of the duty cycle is based on the battery and Vdc1 voltages. As can be seen in the figure, as long as the Vdc1 increases and approximates the Vbat voltage, the duty cycle becomes smaller. This happens because the MPPT system works with a boost topology.

As the 3 scenarios have depicted, the next step is to analyse which of them generates the biggest power peak and the most energy for the four wind gusts. All this information can be seen in Table 7.

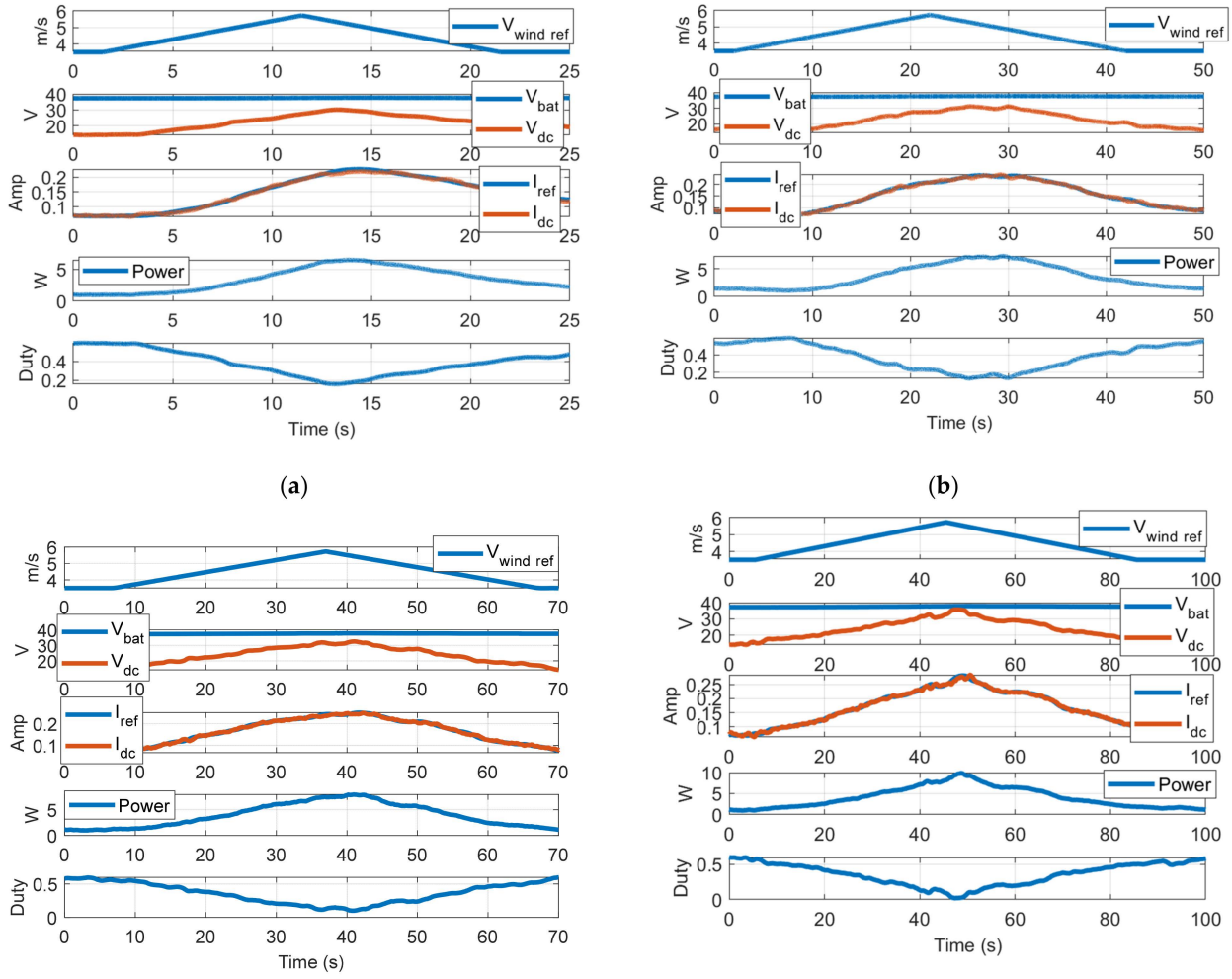

Figure 44. Performance of the Ayanz Wind Turbine with screw blades at variable wind speed tests with MPPT. (**a**) 10 s + 10 s wind gust, (**b**) 20 s + 20 s wind gust, (**c**) 30 s + 30 s wind gust, (**d**) 40 s + 40 s wind gust.

Table 7. Amount of energy generated by each power conversion system configuration at each wind pattern.

	Energy and Peak of Power Generated During the Test		
Wind Speed Pattern	**Only Rectifier**	**Pseudo-MPPT**	**MPPT**
10 s + 10 s wind gust	E = 6.295 J P_{peak} = 9.3 W	E = 8.112 J P_{peak} = 9.59 W	E = 6.13 J P_{peak} = 6.48 W
20 s + 20 s wind gust	E = 12.814 J P_{peak} = 9.62 W	E = 14.88 J P_{peak} = 8.83 W	E = 12.46 J P_{peak} = 7.31 W
30 s + 30 s wind gust	E = 22.204 J P_{peak} = 9.83 W	E = 23.246 J P_{peak} = 10 W	E = 19.96 J P_{peak} = 8 W
40 s + 40 s wind gust	E = 30.874 J P_{peak} = 9.91 W	E = 31.12 J P_{peak} = 10.1 W	E = 29.47 J P_{peak} = 9.87 W

For the scenario presented, the best power conversion system is the pseudo-MPPT; it has the biggest power peaks and the most energy for the four wind gusts. Then, the only rectifier topology has quite good numbers, too. Finally, the MPPT system is the worst of the three, especially in the fast wind gusts (referring to maximum power values).

This may happen since the control slows the system and does not have enough time to follow the wind gust correctly; this can be seen in the last wind gust, where the MPPT approximates the other two topologies. Nevertheless, the energy obtained by the MPPT system is quite equal to that of the other two. Looking at the table in a more general way, it can be said that despite the difference in both analysed values, there is not a very big difference between all of them, especially between the only rectifier and the pseudo-MPPT power conversion system. Hence, paying only attention to the absolute numerical results, it can be concluded that the pseudo-MPPT configuration obtains the best energy generation results of the experimental tests performed (Table 7). Although the MPPT is prepared to maximise the generated power energy at constant wind operation conditions, the variable nature of the wind (gusty winds at city locations) makes the MPPT not able to extract the maximum energy from the wind. This fact occurs mainly due to delays and inaccuracies at the MPPT control loops. On the contrary, pseudo-MPPT and Only-Rectifier configurations, as they do not present control loops, naturally tend to present faster dynamics, adapting quicker the rotational speed to the varying wind gusts and, therefore, being able to generate more power than MPPT configuration in many wind varying circumstances. It is not discardable that different MPPT configurations in different wind turbines, tuned faster and more accurately than what is conducted in the work of this article, would generate more power energy than what is shown here. However, after efforts to improve the MPPT energy generation performance, the authors obtained the best performance.

5.5. Performance at Variable Wind Speed and Turbine Initially Wrongly Oriented to the Wind's Direction

It is important to note that the wind does not always go in the same direction in city locations where there are many obstacles, as depicted in Figure 45. Normally, most of the tests found in the specialised literature tend to assume that the direction of the wind is constant. However, in reality, in cities, the turbulent winds tend to change direction quite fast in a few seconds. This fact ensures the importance of testing the Ayanz wind turbine along the MPPT conversion system with different initial orientations and different wind gusts. In this test, the adaptability and reliability of the Ayanz with turbine to different orientated gusts is evaluated. The tests are not intended to describe exactly the real winds since this would be very difficult to reproduce in a laboratory. Instead, it wants to obtain a rough and basic idea of how much energy is lost in a simplified wind direction variation at the studied Ayanz wind turbine.

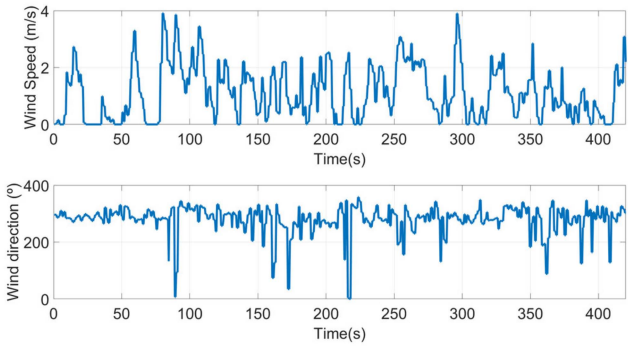

Figure 45. Wind speed and wind speed direction on a low-moderate windy day (Anemometer: WMS-21 Wind Station of Omega manufacturer, with sample time = 0.5 s). During the measurements, the wind's direction is dominantly around 300° (coming from North-West), but during some second intervals, the direction changes quickly dozens of degrees repeatedly.

Figure 46 shows the results obtained for the orientation-changing tests. Two wind gusts have been used for this test: one of 20 s (10 s increasing wind and 10 s decreasing wind) and the other of 100 s (50 s increasing and 50 s decreasing). For each wind gust, two initial orientations were used: 15° wrongly orientated and 45° wrongly orientated.

For a more realistic definition of the test, before starting the test, the Ayanz turbine was already rotating, and when the ramp wind started, the Ayanz turbine was disorientated with the defined degrees for the test. In Figure 46a,b, the results of the 20 s test can be seen. The orientation time for these two is 4 s. The difference between both is that for the Figure 46a case, the Ayanz turbine does not stop rotating because some part of the gust indeed affects the blades. For Figure 46b, as the disorientation angle is much bigger, the Ayanz turbine stops rotating as a result of almost no wind affecting the blades. This fact makes a big difference because, in Figure 46b, the turbine needs to start rotating again, having to surpass the initial inertia to start rotating and having again an initial transitory, which makes big energy lost. The case for Figure 46c,d is quite similar to the previously mentioned. However, it presents some little differences. In this case, the gust lasts 100 s, which makes it much larger. Thus, the same phenomena that happen in the previous case appear in this one. The orientation time is a bit longer, approximately 7 s because the wind speed reference does not grow as fast as in the other case. For Figure 46c, the Ayanz turbine does not stop rotating as in the previous case, and the only energy lost occurs in the first 7 s needed for correct alignment with the wind's direction. Nevertheless, the energy lost is minimal. Conversely, Figure 46d stops rotating during the orientating process, and when it reaches the alignment with the wind, it needs to start up again, making it lose a big amount of energy.

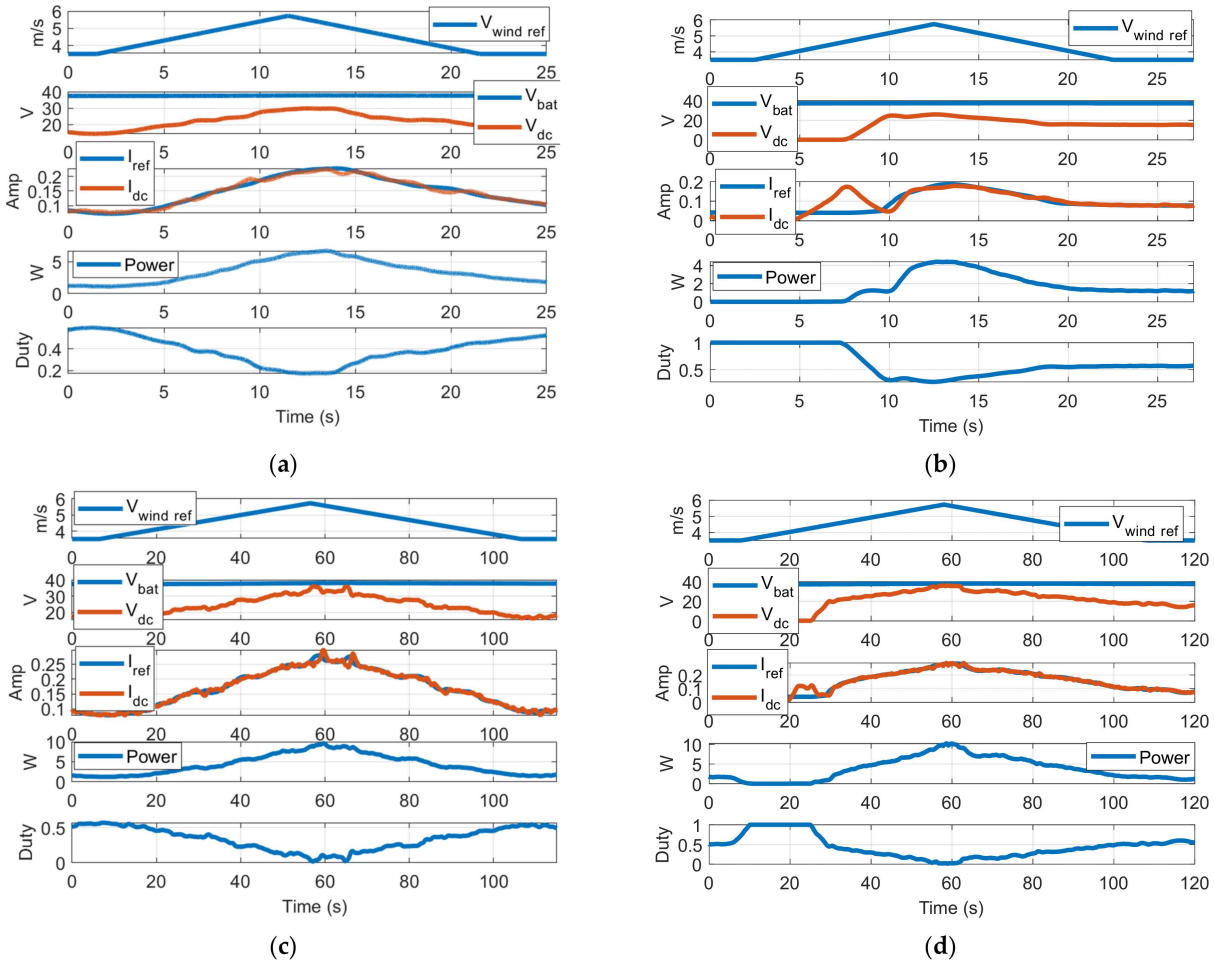

Figure 46. Performance of the Ayanz Wind Turbine with screw blades at variable wind speed tests, with MPPT power conversion system and turbine, initially wrongly oriented. (**a**) 10 s + 10 s wind gust and turbine initially 15° wrongly oriented, (**b**) 10 s + 10 s wind gust and turbine initially 45° wrongly oriented, (**c**) 50 s + 50 s wind gust and turbine initially 15° wrongly oriented, (**d**) 50 s + 0 s wind gust and turbine initially 45° wrongly oriented.

In Table 8, the previously mentioned results are summarised. For the cases of 45° of disorientation compared to their respective wind gust 15° disorientated cases, the generated power peak is smaller, and the total obtained energy is consequently also smaller (check Figure 37 for a simplified representation of theoretical power and energy curves). Hence, this experiment evaluates in a simplified manner the generated energy loss when the wind direction that faces a wind turbine changes. Thus, analysing the power and energy generated at the 'short' 10 s + 10 s wind gust, it is seen that the energy loss is around 55% (2.73 J to 6.08 J) due to a significant initial wrong orientation. Meanwhile, for the 'slow' wind gust of 50 s + 50 s, the energy loss is around 8% (31.8 J to 34.36 J), which is less significant. Hence, although there are losses of energy generation due to the wrong initial orientation of the turbine, these are notorious when the wind gust is fast since the wind turbine dedicates a proportional amount of the wind gust time to obtain the proper orientation (with the vane), not being fully efficient in its objective of energy generation. Therefore, with these results, roughly, it can be said that with the evaluated wind turbine and electronic equipment, at 'fast' wind gusts that change their direction significantly, too, the energy loss can be bigger than 50%. While at 'slow' wind gusts that also change its direction, the energy loss is around 10%, not so dramatic. Consequently, if the wind turbine is placed at a location surrounded, for instance, by walls, buildings and obstacles, the wind will be more turbulent, changing its direction continuously, producing a loss of energy generation that can range from 10% to 50%, compared to a location of the same turbine where the wind is very laminar and not turbulent (without architectural obstacles that produce a change of direction of the wind). In conclusion, it is worth mentioning that this study, which is related to the change of wind direction, has only been addressed during the experimental validation. There are still no clear simulation models that consider wind turbine generation performance under no alignment to the wind directions, so the most accurate way of studying this phenomenon is through experimental validation with real wind turbines. In addition, for future analysis in new papers, it would be interesting to carefully compare the performance of vertical-axis and horizontal-axis wind turbines under changes in wind direction.

Table 8. Amount of energy generated by each orientation at each wind pattern.

Energy and Peak of Power Generated During the Test	
Wind Speed Pattern	**Pseudo-MPPT**
10 s + 10 s wind gust, 15° disoriented	E = 6.08 J P_{peak} = 6.67 W
10 s + 10 s wind gust, 45° disoriented	E = 2.73 J P_{peak} = 4.4 W
50 s + 50 s wind gust, 15° disoriented	E = 34.36 J P_{peak} = 9.63 W
50 s + 50 s wind gust, 45° disoriented	E = 31.84 J P_{peak} = 10.22 W

5.6. Performance at Repetitive Wind Gusts

The following test consists of repetitive wind gusts with no change in its direction. This laboratory test is a simplification of the repetitive wind gusts that can be found in many city areas. For practical reasons, the real winds present in the cities cannot be reproduced with the available wind maker, so this repetitive wind pattern has been used as a simplified approximation of the real winds of the cities. For these tests, the power conversion system that is going to be used is the pseudo-MPPT.

Figure 47 shows the behaviour of the Ayanz turbine at repetitive wind gusts. These gusts were 20 s, 10 s, and 5 s, and for each test, 4 of them were reproduced. The case for Figure 47a is the one where the system reaches the peak power without any trouble and follows the wind reference perfectly. It can be seen that the power peak almost reaches de

10 W for all the gusts. In the case of Figure 47b, the system starts to have issues reaching the maximum power that can be achieved (Figure 47a), reaching 7.5 W in three gusts and 9 W in one of them. It can also be seen that the shapes of the power curves that appear tend to become smoother. For the last case, in Figure 47c, the worst power performance generation curves are obtained. The dynamics of the current and power are so fast that the power peak is reduced substantially, reaching a maximum of 6.5 W for the best case, which makes a big difference with the 10 W it can really extract.

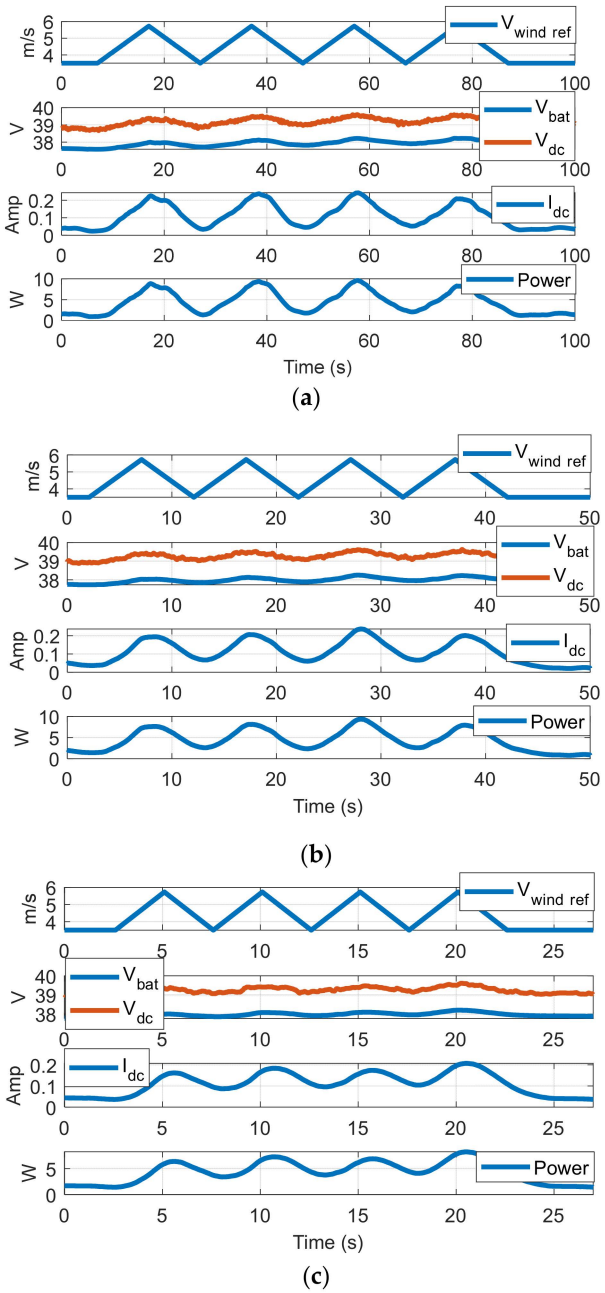

Figure 47. Performance of the Ayanz Wind Turbine with screw blades at repetitive wind gusts tests, with pseudo-MPPT power conversion system with L = 38 mH. (**a**) 10 s + 10 s repetitive wind gust, (**b**) 5 s + 5 s repetitive wind gust, (**c**) 2.5 s + 2.5 s repetitive wind gust.

6. Final Discussion

6.1. Variable Wind Speed Conditions and Turbine Performances

Finally, in this section, a short discussion is provided, taking into consideration the results obtained and shown in the paper. First of all, it has been shown that typical wind

curves provided by manufacturers at steady-state winds [34] are not enough to evaluate the generated energy at city performances. As graphically illustrated in Figure 48, the steady-state power vs. wind speed curves often provided to know the energy production is not sufficient to accurately estimate this energy of small-wind turbines located at places where gusty winds are more common. Considering the small inertias of such types of small turbines, they can often follow quite accurately many dynamics of the wind pattern, providing a proportional extra energy generation than higher power wind turbines (with higher inertias due to their bigger dimensions).

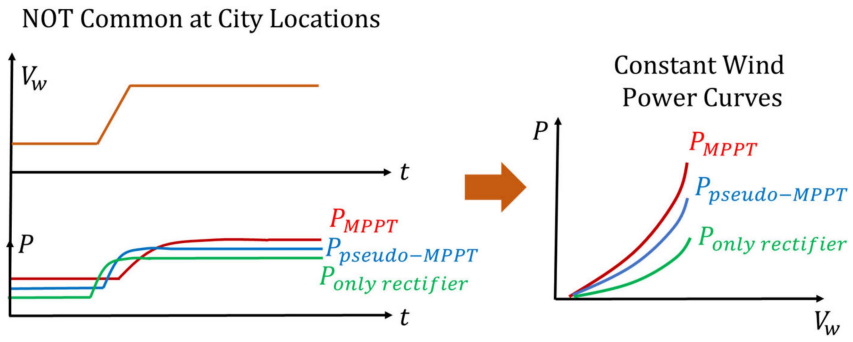

Figure 48. Wind patterns in which constant wind speed is maintained at steady-state and consequent wind-power curves provided by wind turbine manufacturers. Note that these types of wind patterns are not typical at city locations.

Regarding to the most appropriate power conversion system for small-wind turbines, it is difficult to conclude definitively. As observed in simulation and experimental-based analyses performed in previous sections and graphically simplified in Figure 49, there can be many situations and contexts in which a given specific MPPT could be better, or a pseudo-MPPT could be better, or even an Only-Rectifier power conversion topology could be better as well.

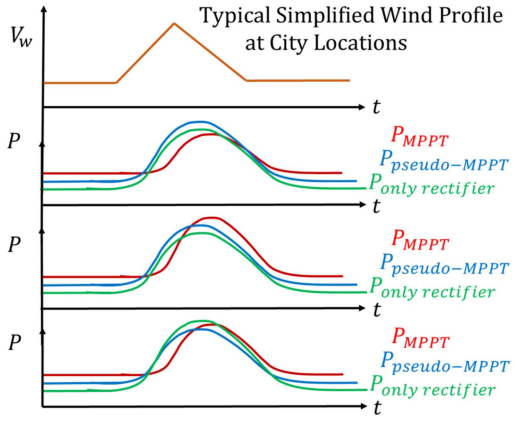

Figure 49. Three possible examples of the power-energy generation situations that can occur with typical simplified 'ramp-based' wind patterns. (There may be many other power-energy generation situations since performances like delay, peak power, time at which the peak power occurs, energy area, and so on, can be different depending on the specific MPPT, pseudo-MPPT and Only-Rectifier analysed).

Depending on many factors, it is not clear whether any of the three studied topologies could be the best at extracting energy from the wind. The most determinant factors could be the ones covered in Table 9.

Table 9. Most determinant factors for maximising the energy extracted from the wind in small-wind turbines.

Main Characteristic to Maximize the Energy Generation
type of wind gusts incident at the wind turbine: slow up-down winds are preferable to be followed by the wind turbine
low inertia of the turbine
non-peaked Cp(λ) curve (wide λ range of high Cp values)
starting-up torque (at zero speed) characteristic of the wind turbine (not studied at this article)
quick orientation of the turbine to the wind changing direction
small parasitic impedances of the electric generator that improves dynamic response
DC bus voltage utilized at the fixed voltage DC side (voltage of battery) according to the wind turbine aerodynamic characteristic in Only-Rectifier and pseudo-MPPT configurations
reduction of electric losses of generator and power conversion system (including microprocessor and sensor's losses at MPPT configuration)
etc.

Finally, Figure 50 shows an example of additional information that could be provided by Small Wind Turbines to be placed at city locations affected by varying wind speeds. This information could complement the typical power vs. wind speed curves provided by manufacturers in order to more accurately know their energy production in a specific location. Thus, with these types of curves, it will be possible to know how much energy extracts a specific wind turbine under wind gusts of different durations, knowing easily if the turbine has been designed to reasonably follow such kinds of wind gusts.

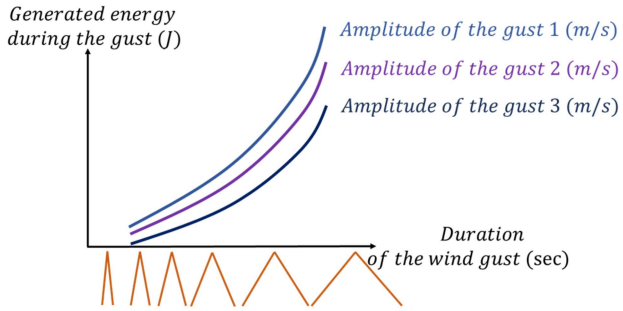

Figure 50. Additional information that could be provided by small wind turbines (normally present much smaller inertia than high-power three-bladed wind turbines) should be placed at city locations with varying wind speeds.

6.2. Inertia Comparison of Different Wind Turbines

In this sub-section, an approximative inertia evaluation of the most relevant small wind turbine morphologies is carried out. There is an uncountable amount of wind turbine topologies on the market, but only the most typical and relevant ones will be studied for this inertia evaluation analysis. Thus, an approximated inertia equation is provided for the four wind turbine morphologies studied based on the geometrical dimensions of the turbine as well as the density of the material used for the blade's materialisation. For simplicity, several assumptions and simplifications are made so the obtained mathematical expressions for the inertia values are sufficiently simple and manageable. Basically, the main assumption is that the blade shape or geometry is simplified to a 'similar' shape in which the inertia expression is well known already. Then also, only blades are considered in the inertia calculation, while other elements necessary for their assembly are neglected: shafts, hubs, screws and tie rods, etc. The small-wind turbines are considered to present

three blades for equal comparative purposes. However, a different number of blades can also be evaluated using the expressions derived.

Hence, the first small wind turbine considered is obviously, the one utilised in this paper, i.e., the Ayanz wind turbine with screw blades. As has been shown, the screw blades utilised in the analysis of the paper are the Spiral Archimedes shape [22,23,30]. Figure 51 illustrates a simplified representation of one of the blades and the equivalent inertia expression derived. Note again that the shaft is ideally considered with zero radio, which implies that the blade starts at zero angle θ.

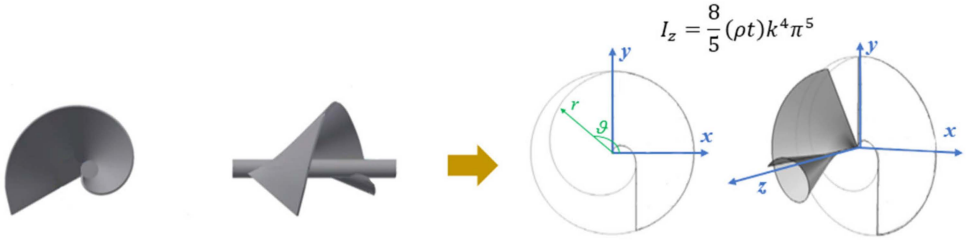

Figure 51. Simplified representation of a Spiral Archimedes blade in a 3-Bladed Horizontal axis Ayanz Wind Turbine with screw blades.

In polar coordinates, the radio of the spiral blade projection at the x-y plane can be expressed as [30]:

$$r = k \cdot \theta \tag{6}$$

Being k, a real number. By changing the parameter k, the distance between loops is modified. Here, it is assumed that the mass particles of the blade projected to the x-y plane, resulting in the Archimedean Spiral, present the same distance to the z-axis as the original three-dimensional blade mass particles. Then, the differential mass is derived as [37]:

$$dm = (\rho t)dA = (\rho t)(rdrd\theta) \tag{7}$$

With ρ the density of the material employed and t, the thickness of the blade.

$$I_z = \int_0^{k\theta} r^2 dm = \int_0^{k\theta}\int_0^{2\pi} r^2(\rho t)(rdrd\theta) \tag{8}$$

Which results in:

$$I_z = \frac{8}{5}(\rho t)k^4\pi^5 \tag{9}$$

Thus, for this type of blade geometry, the highest ratio of the spiral determined by k, the maximum angle 2π ($r = k \cdot 2\pi$) and the density ρ determines the inertia of one of the blades. Then, in order to calculate the total inertia of the 3 blades, this value must be simply multiplied by 3.

Then the second type of wind turbine considered is the classic horizontal axis 3-bladed wind turbine. At this time, the geometry of the complex geometry of an airfoiled profile is simplified to a rectangular prism of thickness t, as depicted in Figure 52. It can be considered as a family of wind turbines, depending on the number of blades employed.

In this case, the equivalent inertia across the z axis of a rectangular prism geometry is of common knowledge and is equal to [37]:

$$I_z = (\rho t)(ab)\left(\frac{1}{12}b^2 + \frac{1}{3}a^2\right) \tag{10}$$

Again, in order to calculate the total inertia of the 3 blades, this value should be simply multiplied by 3.

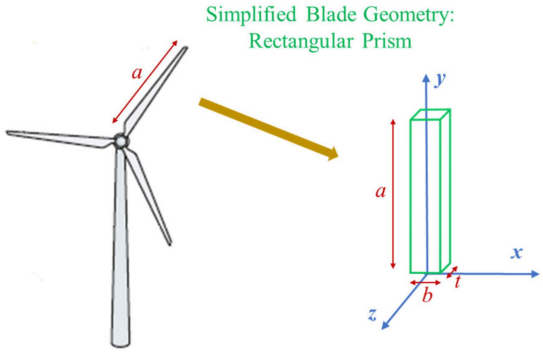

$$I_z = (\rho t)(ab)(\tfrac{1}{12}b^2 + \tfrac{1}{3}a^2)$$

Figure 52. Simplified representation of a horizontal axis 3-bladed wind turbine.

Then, in Figure 53, the 3rd type of small wind turbine morphology is illustrated. It is a vertical axis 3-bladed Darrieus-type wind turbine, first patented a century ago by Darrieus [38]. For simplicity, and because many commercial turbines of this type operate in this way, the curvature or oval shape of the blades has not been considered. Hence, as can be noticed in Figure 53, the complex geometry of an airfoiled profile is again simplified to a rectangular prism of thickness *t*.

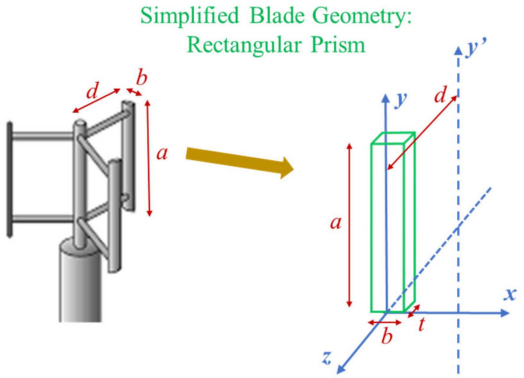

$$I_{y'} = (\rho t)(ab)(\tfrac{1}{12}b^2 + \tfrac{1}{12}t^2 + d^2)$$

Figure 53. Simplified representation of a vertical axis 3-bladed Darrieus type wind turbine.

In this case, again as before, the equivalent inertia across the y-axis of such a simple geometry is of common knowledge and is equal to [37]:

$$I_y = \frac{1}{12}(\rho t)(ab)(b^2 + t^2) \tag{11}$$

While the inertia across the parallel axis y', by using the Steiner theorem is [37]:

$$I_{y'} = (\rho t)(ab)\left(\frac{1}{12}b^2 + \frac{1}{12}t^2 + d^2\right) \tag{12}$$

Note that the distance *d* to the shaft, strongly affects to the inertia compared to the other two parameters *b* and *t*, which are divided by a factor of 12. This is due to the fact that all the mass of the blade is concentrated to a distance d to the shaft. So, if this distance is 'high', the tendency of the equivalent inertia will be 'high' as well.

Finally, the last family of small wind turbines is named Vertical Axis Ayanz-Savonious wind turbines, being consequent with their corresponding respective patents of XVII century (Ayanz- [18]) and XX century (Savonius- [39]). In Figure 54, a simplified representation

of a vertical axis 3-bladed wind turbine of this type is depicted. The blades are placed at a distance from the shaft (more like in the Ayanz patent rather than in the Savonious patent). In this case, the geometry of the blades is half cylinders of internal and external radios R1 and R2.

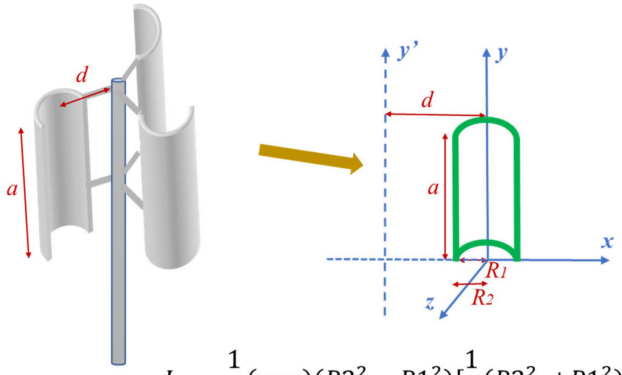

$$I_{y\prime} = \frac{1}{2}(\rho\pi a)(R2^2 - R1^2)[\frac{1}{2}(R2^2 + R1^2) + d^2]$$

Figure 54. Simplified representation of a Vertical Axis Ayanz-Savonious 3-Bladed wind turbine (* Note that the Savonious patent and Ayanz patent present differences, but the most relevant one is that the Savonious patent considers an embrace of the blades to the central shaft, while in Ayanz patent, the blades are fixed with rods to a distance of the shaft).

Thus, again, as in the previous case, the equivalent inertia across the y-axis of such a simple geometry is of common knowledge and is equal to [37]:

$$I_y = \frac{1}{4}(\rho\pi a)\left(R2^4 - R1^4\right) \tag{13}$$

While again, the inertia across the parallel axis y', by using the Steiner theorem is [37]:

$$I_{y\prime} = \frac{1}{2}(\rho\pi a)\left(R2^2 - R1^2\right)\left[\frac{1}{2}\left(R2^2 + R1^2\right) + d^2\right] \tag{14}$$

In this particular case, the distance d compared with other parameters $R1$ and $R2$ do not increase the inertia so dramatically as in previous Darrieus type turbines, since the mass of the blades is distributed across the distance $d - R2$ to d + $R2$.

Finally, a quantitative comparison is carried out for the four types of small wind turbines previously modelled. It is almost impossible to perform a fair comparison between four different morphologies of turbines, so the results have to be taken with caution or at least comprehensively. Thus, the comparative framework adopted considers an equal area of wind incidence for each wind turbine. This means that for the horizontal axis wind turbines, a circular area of incidence of the air is considered, while for the vertical axis wind turbines, a rectangular area is considered. Table 10 shows the areas, proportions and values that have been considered.

It is noticed that each wind turbine presents different thicknesses and proportions of geometries. It has been treated to be as close to a realistic, practical design as possible. Nevertheless, if the reader wants to use different parameters and proportions, all the mathematical formulations can be adapted. It has to be remarked that for the Ayanz-Savonious vertical axis wind turbine, the proportions considered are as proposed in the original Ayanz patent [18]. Hence, four different incident wind areas are considered and applied to the 4 wind turbines with proportions and parameter values in Table 10. The resulting inertia is provided in Figure 55.

Table 10. Wind incident areas, proportions and parameter values have been considered for each wind turbine. Material of the blades: aluminium, density = 2700 kg/m^3.

	Incident Wind Area	***t* (m)**	**-**	**-**
Ayanz Wind Turbine with screw blades $\boldsymbol{I_z = \frac{8}{5}(\rho t)k^4\pi^5}$	$\pi(k \cdot 2\pi)^2$	0.003	-	-
	Incident Wind Area	***t* (m)**	**b**	**-**
Horizontal Axis 3-Bladed $\boldsymbol{I_z = (\rho t)(ab)\left(\frac{1}{12}b^2+\frac{1}{3}a^2\right)}$	$\pi(a)^2$	0.009	$0.2a$	-
	Incident Wind Area	***t* (m)**	**b**	**d**
Vertical Axis 3-Bladed Darrieus $\boldsymbol{I_{y'} = (\rho t)(ab)\left(\frac{1}{12}b^2+\frac{1}{12}t^2+d^2\right)}$	$2da$	0.006	$0.2a$	$(1/3)a$
	Incident Wind Area	***t* (m)**	**d**	**a**
Vertical Axis 3-Bladed Ayanz-Savonius $\boldsymbol{I_{y'} = \frac{1}{2}(\rho\pi a)(R2^2-R1^2)\left[\frac{1}{2}(R2^2+R1^2)+d^2\right]}$	$2a(d+R2)$	0.003	$2R2$	$2(d+R2)$

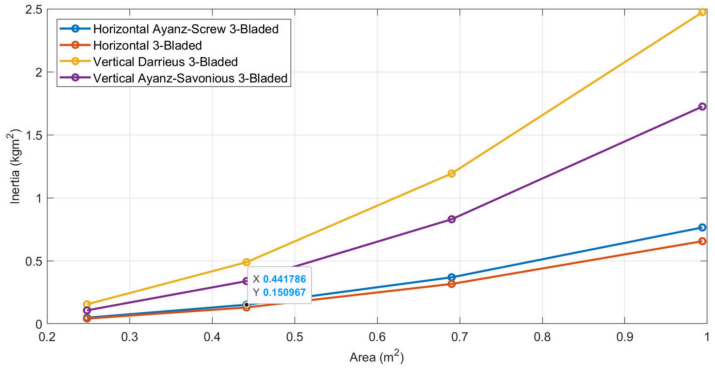

Figure 55. Inertias were evaluated according to the simplified expressions provided, considering equal wind incident areas in four wind turbines. Areas (m^2): [0.24,0.44,0.69,0.99].

It can be noticed that the vertical axis wind turbines present higher inertia than the horizontal axis ones, and this difference becomes greater with higher areas. This is due to the fact that the majority mass of their blades is concentrated around a distance d to the shaft. If different proportions and geometrical values are used, the resulting inertia would change. However, this is a reasonably good first approach to better understand the intrinsic natural inertia values of different wind turbines.

6.3. General Qualitative Performance of Different Small Wind Turbines

To conclude, this section provides a comparison of the general qualitative performance of different wind turbines. Table 11 shows the performance of several objectives that should seek different wind turbine designs. The most commonly used small wind turbines have been classified into 4 four main groups as in the previous sub-section. It can be noticed that the Ayanz Wind Turbine with screw blades employed in this article is very well positioned among typical small wind turbines. Thus, in terms of maximum achievable Cpmax, probably the horizontal axis with airfoiled blades is the best, then would come the Darrieus type turbines, then the Ayanz with screw blades and finally the drag type vertical axis ones. However, as has been shown in this article, this Cpmax alone is not the most determinant factor in maximising the generated energy. This factor should be accompanied by a low inertia of the wind turbine. As has been shown, in principle, the inertia of vertical-axis wind turbines is higher than that of horizontal-axis ones. Then, the electric losses of the turbine depend only on the electronic conversion system used and do not depend on the turbine's geometry. The peaked shape of the Cp(λ) curve is an issue

that could not be studied in this article due to a lack of information. Regarding the start-up torque characteristic, probably the drag type vertical axis ones and Ayanz with screw blades could be the best. In relation to the maximisation of the generated energy at winds that often change direction, the vertical axis wind turbines are well positioned. Probably the horizontal axis with airfoiled blades presents the worst performance since the vane is normally located behind the blades, and therefore, they are moved by de-energized winds in comparison with the Ayanz with screw blades. Consequently, taking into consideration all these indicators, the horizontal axis wind turbines (screw and airfoiled blades) probably are the best positioned to maximise the energy production and capacity factor under gusty winds of city locations. Then, the Ayanz with screw blades is clearly the best positioned in minimisation the visual impact and acoustic noise, minimisation of birds' casualties and safety in case of blade failure. On the contrary, the worst positions in these last four indicators are horizontal axis turbines with airfoiled blades.

Table 11. General Qualitative Performance of Different Small Wind Turbines. Best mark: ++, second mark: +, third mark: -, worst mark: --.

Objective	**Drag Type Vertical Axis Ayanz-Savonius** 	**Ayanz with Screw Blades** 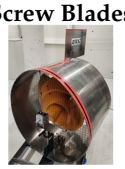	**Vertical Axis Darrieus** 	**Horizontal Axis** 
Maximize energy production at gusty winds of cities or Maximize the Capacity Factor (It is necessary to maximize the following indicators)	+	++	+	++
- High C_{pmax} natural characteristic	-	+	+	++
- Low inertia	-	+	-	+
- Non-peaked Cp(λ) curve	Not clear	Not clear	Not clear	Not clear
- Reduction of electric losses	+	+	+	+
- Maximize the generated energy at low-speed winds (good start-up torque characteristic)	+	+	-	-
- Maximize the generated energy at winds that change often the direction (quick orientation for horizontal axis turbines)	++	+	++	-
Minimize the visual impact (mainly avoid seeing the blades rotating)	+	++	-	--
Minimize the acoustic noise impact (minimize noise due to fast rotations of blades)	+	+	-	--
Maximize prevention of birds' deaths	+	++	-	-
Maximize safety in case of destructive failure of blades	-	++	--	--
Maximize reliability of the Wind Turbine (low mechanical stress due to low rotational speed and Blades are protected from rain)	+	++	+	+

Author Contributions: Conceptualization, G.A. and A.P.; methodology, G.A.; software, G.A., A.P. and G.K.; validation, A.P., G.A. and G.K.; formal analysis, A.P., G.A. and G.K.; investigation, G.A. and A.P.; resources, G.A.; data curation, A.P.; writing—original draft preparation, G.A. and A.P.; writing—review and editing, G.A. and A.P.; visualisation, G.A. and A.P.; supervision, G.A.; project administration, G.A.; funding acquisition, G.A. All authors have read and agreed to the published version of the manuscript.

Funding: This research was partially founded by the Basque Government's program supporting Research Groups of the Basque University System, conducted by the Education Department (2022–2025).

Data Availability Statement: Restrictions apply to the dataset.

Conflicts of Interest: The authors declare no conflict of interest.

References

1. Buri, Z.; Sipos, C.; Szűcs, E.; Máté, D. Smart and Sustainable Energy Consumption: A Bibliometric Review and Visualization. *Energies* **2024**, *17*, 3336. [CrossRef]
2. Wardal, W.J.; Mazur, K.; Barwicki, J.; Tseyko, M. Fundamental Barriers to Green Energy Production in Selected EU Countries. *Energies* **2024**, *17*, 3664. [CrossRef]
3. Zidane, T.E.; Aziz, A.L.; Zahraoui, Y.; Kotb, H.; AboRas, K.M.; Kitmo; Jember, Y.B. Grid-Conecctd Solar PV Power Plants Optimization: A Review. *IEEE Access* **2023**, *11*, 79588–79608. [CrossRef]
4. Pater, S. Increasing Energy Self-Consumption in Residential Photovoltaic Systems with Heat Pumps in Poland. *Energies* **2023**, *16*, 4003. [CrossRef]
5. Liu, H.-Y.; Skandalos, N.; Braslina, L.; Kapsalis, V.; Karamanis, D. Integrating Solar Energy and Nature-Based Solutions for Climate-Neutral Urban Environments. *Solar* **2023**, *3*, 382–415. [CrossRef]
6. Boudjemai, H.; Ardjoun, S.A.E.M.; Chafouk, H.; Denai, M.; Elbarbary, Z.M.S.; Omar, A.I.; Mahmoud, M.M. Application of a Novel Synergetic Control for Optimal Power Extraction of a Small-Scale Wind Generation System with Variable Loads and Wind Speeds. *Symmetry* **2023**, *15*, 369. [CrossRef]
7. Stepaniuk, V.; Pillai, J.R.; Bak-Jensen, B.; Padmanaban, S. Estimation of Energy Activity and Flexibility Range in Smart Active Residential Building. *Smart Cities* **2019**, *2*, 471–495. [CrossRef]
8. Ramadan, R.; Huang, Q.; Zalhaf, A.S.; Bamisile, O.; Li, J.; Mansour, D.-E.A.; Lin, X.; Yehia, D.M. Energy Management in Residential Microgrid Based on Non-Intrusive Load Monitoring and Internet of Things. *Smart Cities* **2024**, *7*, 1907–1935. [CrossRef]
9. Mortensen, L.K.; Shaker, H.R. Data-Driven Reliability Prediction for District Heating Networks. *Smart Cities* **2024**, *7*, 1706–1722. [CrossRef]
10. Hammoumi, L.; Maanan, M.; Rhinane, H. Characterizing Smart Cities Based on Artificial Intelligence. *Smart Cities* **2024**, *7*, 1330–1345. [CrossRef]
11. Lazaroiu, A.C.; Gmal Osman, M.; Strejoiu, C.-V.; Lazaroiu, G. A Comprehensive Overview of Photovoltaic Technologies and Their Efficiency for Climate Neutrality. *Sustainability* **2023**, *15*, 16297. [CrossRef]
12. Pu, O.; Yuan, B.; Li, Z.; Bao, T.; Chen, Z.; Yang, L.; Qin, H.; Li, Z. Research on the Characteristics of Urban Building Cluster Wind Field Based on UAV Wind Measurement. *Buildings* **2023**, *13*, 3109. [CrossRef]
13. Corbalán, P.A.; Chiang, L.E. Fast Power Coefficient vs. Tip–Speed Ratio Curves for Small Wind Turbines with Single-Variable Measurements following a Single Test Run. *Energies* **2024**, *17*, 1199. [CrossRef]
14. Ramos-Paja, C.A.; Henao-Bravo, E.E.; Saavedra-Montes, A.J. MPPT Solution for Commercial Small Wind Generation Systems with Grid Connection. *Energies* **2023**, *16*, 719. [CrossRef]
15. Zagubień, A.; Wolniewicz, K. Energy Efficiency of Small Wind Turbines in an Urbanized Area—Case Studies. *Energies* **2022**, *15*, 5287. [CrossRef]
16. Rosato, A.; Perrotta, A.; Maffei, L. Commercial Small-Scale Horizontal and Vertical Wind Turbines: A Comprehensive Review of Geometry, Materials, Costs and Performance. *Energies* **2024**, *17*, 3125. [CrossRef]
17. Castillo, O.C.; Andrade, V.R.; Rivas, J.J.R.; González, R.O. Comparison of Power Coefficients in Wind Turbines Considering the Tip Speed Ratio and Blade Pitch Angle. *Energies* **2023**, *16*, 2774. [CrossRef]
18. Abad, G.; Zarketa-Astigarraga, M.P.Y.A. *Molinos de Viento Patentados por Jerónimo de Ayanz y Beaumont en el año 1606*; un Análisis Conceptual Desde una Perspectiva Ingenieril del Año 2021; Mondragon Unibertsitatea: Mondragon, Spain, 2021.
19. Tapia, N.G. *Jerónimo de Ayanz y Beaumont. Un Inventor Navarro (1553–1613)*; Universidad Pública de Navarra: Pamplona, Spain, 2010.
20. Liam F1 Archimedes AWM-750D-150W Datasheet. (Liam F1 Archimedes). Available online: https://thearchimedes.com/ (accessed on 27 October 2024).
21. Song, K.; Huan, H.; Kang, Y. Aerodynamic Performance and Wake Characteristics Analysis of Archimedes Spiral Wind Turbine Rotors with Different Blade Angle. *Energies* **2023**, *16*, 385. [CrossRef]
22. Refaie, A.G.; Hameed, H.A.; Nawar, M.A.; Attai, Y.A.; Mohamed, M.H. Comparative investigation of the aerodynamic performance for several Shrouded Archimedes Spiral Wind Turbines. *Energy* **2021**, *239*, 122295. [CrossRef]

23. Kim, K.; Ji, K.; Kim, H.Y.; Lu, Q.; Baek, J. Experimental and Numerical Study of the Aerodynamic Characteristics of an Archimedes Spiral Wind Turbine Blade. *Energies* **2014**, *7*, 7893–7914. [CrossRef]
24. Refaie, A.G.; Hameed, H.A.; Nawar, M.A.; Attai, Y.A.; Mohamed, M.H. Qualitative and quantitative assessments of an Archimedes Spiral Wind Turbine performance augmented by a concentrator. *Energy* **2021**, *231*, 121128. [CrossRef]
25. Jang, H.; Kim, D.; Hwang, Y.; Paek, I.; Kim, S.; Baek, J. Analysis of Archimedes Spiral Wind Turbine Performance by Simulation and Field Test. *Energies* **2019**, *12*, 4624. [CrossRef]
26. Arzuaga, A.; Estivariz, A.; Fernández, O.; Gubía, K.; Plaza, A.; Abad, G.; Cabezuelo Romero, D. Low-Cost Maximum Power Point Tracking Strategy and Protection Circuit Applied to an Ayanz Wind Turbine with Screw Blades. *Energies* **2023**, *16*, 6204. [CrossRef]
27. Micallef, D.; Van Bussel, G. A Review of Urban Wind Energy Research: Aerodynamics and Other Challenges. *Energies* **2018**, *11*, 2204. [CrossRef]
28. Marrone, P.; Fiume, F.; Laudani, A.; Montella, I.; Palermo, M.; Fulginei, F.R. Distributed Energy Systems: Constraints and Opportunities in Urban Environments. *Energies* **2023**, *16*, 2718. [CrossRef]
29. Krasniqi, G.; Dimitrieska, C.; Lajqi, S. Wind Energy Potential in Urban Area: Case study Prishtina. *Int. J. Technol.* **2022**, *13*, 458–472. [CrossRef]
30. Article from Wikipedia. Available online: https://en.wikipedia.org/wiki/Archimedean_spiral (accessed on 27 October 2024).
31. Njiri, J.G.; Söffker, D. State-of-the-art in wind turbine control: Trends and challenges. *Renew. Sustain. Energy Rev.* **2016**, *60*, 377–393. [CrossRef]
32. Abad, G.; Lopez, J.; Rodriguez, M.; Marroyo, L.; Iwanski, G. *Doubly Fed Induction Machine: Modelling and Control for Wind Energy Generation*; Wiley-IEEE Press: New York, NY, USA, 2011; ISBN 9780470768655.
33. Wu, B.; Lang, Y.; Zargari, N.; Kouro, S. *Power Conversion and Control of Wind Energy Systems*; Wiley-IEEE Press: New York, NY, USA, 2011; ISBN 978-1-118-02899-5.
34. *IEC 61400-1:2019*; Wind Energy Generation Systems—Part 1: Design Requirements. IEC: Geneva, Switzerland, 2019.
35. Amenedo, J.L.R. *Sistemas eólicos de Producción de Energía Eléctrica*; Rueda SL: Valladolid, Spain, 2003; ISBN 8472071391.
36. Camblong, H. Experimental evaluation of wind turbines maximum power point tracking controllers. *Energy Convers. Manag.* **2006**, *47*, 2846–2858. [CrossRef]
37. Beer, F.P. *Vector Mechanics for Engineers. Statics and Dynamics*; Mc Graw Hill: New York, NY, USA, 1995; ISBN 978-0-07-339824-2.
38. Darrieus, G.J.M. Turbine Having Its Rotating Shaft Transverse to the Flow of the Current. U.S. Patent US1835018 1925.
39. Savonius, S.J. Wind Rotor. U.S. Patent US311793 1930.

Disclaimer/Publisher's Note: The statements, opinions and data contained in all publications are solely those of the individual author(s) and contributor(s) and not of MDPI and/or the editor(s). MDPI and/or the editor(s) disclaim responsibility for any injury to people or property resulting from any ideas, methods, instructions or products referred to in the content.